Inorg. Chem. **2006**, *45*, 7877–7890

Electronic Structure of Mononuclear Bis(1,2-diaryl-1,2-ethylenedithiolato)iron Complexes Containing a Fifth Cyanide or Phosphite Ligand: A Combined Experimental and Computational Study

Apurba K. Patra,[†] Eckhard Bill,[†] Eberhard Bothe,[†] Krzysztof Chlopek,[†] Frank Neese,[†] Thomas WeyhermUller,[†] Keira Stobie,[‡] Michael D. Ward,[§] Jon A. McCleverty,[‡] and Karl Wieghardt*,[†]

Max-Planck-Institut für Bioanorganische Chemie, Stiftstrasse 34-36, D-45470 Mülheim an der Ruhr, Germany, School of Chemistry, University of Bristol, Bristol BS8 1TS, U.K., and Department of Chemistry, University of Sheffield, Sheffield S3 7HF, U.K.

Received June 27, 2006

A series of mononuclear square-based pyramidal complexes of iron containing two 1,2-diaryl-ethylene-1,2-dithiolate ligands in various oxidation levels has been synthesized. The reaction of the dinuclear species $[Fe^{III}_2(^1L^{\bullet})_2(^1L)_2]^0$, where $(^1L)^{2-}$ is the closed shell di-(4-*tert*-butylphenyl)-1,2-ethylenedithiolate dianion and $(^1L^{\bullet})^{1-}$ is its one-electron-oxidized π-radical monoanion, with $[N(n\text{-}Bu)_4]CN$ in toluene yields dark green crystals of mononuclear $[N(n\text{-}Bu)_4][Fe^{II}(^1L^{\bullet})_2(CN)]$ (**1**). The oxidation of **1** with ferrocenium hexafluorophosphate yields blue $[Fe^{III}(^1L^{\bullet})_2(CN)]$ (**1**^{ox}), and analogously, a reduction with $[Cp_2Co]$ yields $[Cp_2Co][N(n\text{-}Bu)_4][Fe^{II}(^1L^{\bullet})(^1L)(CN)]$ (**1**^{red}); oxidation of the neutral dimer with iodine gives $[Fe^{III}(^1L^{\bullet})_2I]$ (**2**). The dimer reacts with the phosphite $P(OCH_3)_3$ to yield $[Fe^{II}(^1L^{\bullet})_2\{P(OCH_3)_3\}]$ (**3**), and $[Fe^{III}_2(^3L^{\bullet})_2(^3L)_2]$ reacts with $P(OC_6H_5)_3$ to give $[Fe^{II}(^3L^{\bullet})_2\{P(OC_6H_5)_3\}]$ (**4**), where $(^3L)^{2-}$ represents 1,2-diphenyl-1,2-ethylenedithiolate(2–). Both **3** and **4** were electrochemically one-electron oxidized to the monocations **3**^{ox} and **4**^{ox} and reduced to the monoanions **3**^{red} and **4**^{red}. The structures of **1** and **4** have been determined by X-ray crystallography. All compounds have been studied by magnetic susceptibility measurements, X-band EPR, UV–vis, IR, and Mössbauer spectroscopies. The following five-coordinate chromophores have been identified: (a) $[Fe^{III}(L^{\bullet})_2X]^n$, X = CN^-, I^- (n = 0) (**1**^{ox}, **2**); X = $P(OR)_3$ (n = 1+))**3**^{ox}, **4**^{ox}) with $S_t = {}^1/_2$, $S_{Fe} = {}^3/_2$; (b) $[Fe^{II}(L^{\bullet})_2X]^n$, X = CN^-, (n = 1–) (**1**); X = $P(OR)_3$ (n = 0) (**3**, **4**) with $S_t = S_{Fe} = 0$; (c) $[Fe^{II}(L^{\bullet})(L)X]^n \leftrightarrow [Fe^{II}(L)(L^{\bullet})X]^n$, X = CN^- (n = 2–) (**1**^{red}); X = $P(OR)_3$ (n = 1–) (**3**^{red}, **4**^{red}) with $S_t = {}^1/_2$, $S_{Fe} = 0$ (or 1). Complex **1**^{ox} displays spin crossover behavior: $S_t = {}^1/_2 \leftrightarrow S_t = {}^3/_2$ with intrinsic spin-state change $S_{Fe} = {}^3/_2 \leftrightarrow S_{Fe} = {}^5/_2$. The electronic structures of **1** and **1**^{ox} have been established by density functional theoretical calculations: $[Fe^{II}(^1L^{\bullet})_2(CN)]^{1-}$ (S_{Fe} = 0, S_t = 0) and $[Fe^{III}(^1L^{\bullet})_2(CN)]^0$ ($S_{Fe} = {}^3/_2$, $S_t = {}^1/_2$).

Introduction

Holm and Balch[1a,b,c] reported that the dimeric complexes $[Fe_2(S_2C_2R_2)_4]^z$ (R = CF_3; z = 0, 1−, 2−; R = −CN, z = 2−) undergo a cleavage reaction in the presence of phosphines, arsines, and phosphites, $P(OR)_3$, to yield monomeric five-coordinate complexes $[Fe(S_2C_2R_2)_2L]^z$ (z = 0, 1−). Subsequently, McCleverty and co-workers have synthesized a large number of such species:[2−4] they determined their electronic ground states, measured their electronic spectra,[2−5] and in some cases, they measured their X-band EPR and, later, their Mössbauer spectra.[6,7] Dance et al.[8] synthesized a

* To whom correspondence should be addressed. E-mail: wieghardt@mpi-muelheim.mpg.de.
† Max-Planck-Institut für Bioanorganische Chemie.
‡ University of Bristol.
§ University of Sheffield.

(1) (a) Balch, A. L. *Inorg. Chem.* **1967**, *6*, 2158. (b) Balch, A. L.; Dance, I. G.; Holm, R. H. *J. Am. Chem. Soc.* **1968**, *90*, 1139. (c) Balch, A. L.; Holm, R. H. *Chem. Commun.* **1966**, 552.
(2) McCleverty, J. A.; Atherton, N. M.; Connelly, N. G.; Winscom, C. J. *J. Chem. Soc. A* **1969**, 2242.
(3) McCleverty, J. A.; Ratcliff, B. *J. Chem. Soc. A* **1970**, 1631.
(4) McCleverty, J. A.; Orchard, D. G. *J. Chem. Soc. A* **1971**, 626.
(5) McCleverty, J. A.; Atherton, N. M.; Locke, J.; Wharton, E. J.; Winscom, C. J. *J. Am. Chem. Soc.* **1967**, *89*, 6082.
(6) Birchall, T.; Greenwood, N. N.; McCleverty, J. A. *Nature* **1967**, *215*, 625.

10.1021/ic061171t CCC: $33.50
Published on Web 08/10/2006

Scheme 1. Ligands, Oxidation Levels, Abbreviations, Synthesized Complexes, Their Labels, Overall Spin States, and Intrinsic Iron Ion Spin States.

Ligands:

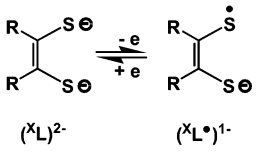

R =	X
	1
	2
	3

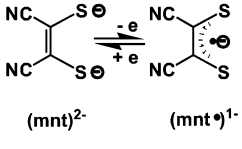

Complex		S_t [a]	S_{Fe} [b]
$[N(n\text{-}Bu)_4][Fe^{II}(^1L^{\bullet})_2(CN)]$	1	0	0
$[Fe^{III}(^1L^{\bullet})_2(CN)]$	1^{ox}	1/2⇌3/2	3/2⇌5/2
$[N(n\text{-}Bu)_4][Cp_2Co][Fe^{II}(^1L^{\bullet})(^1L)(CN)]$	1^{red}	1/2	0 (or 1)
$[Fe^{III}(^1L^{\bullet})_2I]$	2	1/2	3/2
$[Fe^{II}(^1L^{\bullet})_2\{P(OCH_3)_3\}]$	3	0	0
$[Fe^{II}(^3L^{\bullet})_2\{P(OPh)_3\}]$	4	0	0

a) Electronic ground state of complex; *b)* intrinsic spin state of iron ion.

series of $[N(n\text{-}Bu)_4][Fe^{III}(mnt)_2L]$ complexes where L represents an amine such as ammonia or pyridine and $(mnt)^{2-}$ is the maleonitriledithiolate(2−) dianion. These mononuclear complexes possess an intermediate-spin ferric ion ($S_{Fe} = {}^3/_2$), differing in this respect from the monoanions $[Fe(mnt)_2(PR_3)]^-$ which possess an $S_t = {}^1/_2$ ground state and which have been assigned an intrinsic spin state of the central iron ion as low spin ($S_{Fe} = {}^1/_2$).[3] A few diamagnetic, neutral species have been structurally characterized, namely, $[Fe(S_2C_2(CF_3)_2\{AsPh_3\}]$,[9] $[Fe(S_2C_2Ph_2)_2\{P(OCH_3)_3\}]$,[10] and $[Fe(mnt)_2\{2(p\text{-pyridine})\text{-}4,4,5,5\text{-}tetramethylimidazolinium\}]$.[11,12] Many of these mononuclear complexes have been shown electrochemically to be members of an electron-transfer series, eq 1[1−5]

$$[FeL_2X]^{n-2} \underset{-e}{\overset{+e}{\rightleftharpoons}} [FeL_2X]^{n-1} \underset{-e}{\overset{+e}{\rightleftharpoons}} [FeL_2X]^{n} \qquad (1)$$

where, if X is a monoanionic ligand, $n = 0$, and if X is a neutral ligand, $n = +1$.

Although it has been well recognized that dithiolene ligands belong to the redox-noninnocent class of ligands[13] which can exist in at least two different oxidation levels, as shown in Scheme 1, a definitive description of the electronic structure of the above mononuclear iron complexes has not been attempted.[11] For example, the neutral phosphine complex $[Fe(^3L)_2\{PR_3\}]$ may contain (a) two closed-shell dithiolate dianions and an iron(IV) ion ($S_t = 1$ or 2) or (b) one monoanionic π radical ligand, $(^3L^{\bullet})^{1-}$, and one dianionic $(^3L)^{2-}$ ligand yielding the electron distribution $[Fe^{III}(^3L^{\bullet})(^3L)\{PR_3\}] \leftrightarrow [Fe^{III}(^3L)(^3L^{\bullet})\{PR_3\}]$ with an intrinsic high-spin ($S_{Fe} = {}^5/_2$), intermediate-spin ($S_{Fe} = {}^3/_2$), or even low-spin ($S_{Fe} = {}^1/_2$) central ferric ion which would be antiferromagnetically coupled to the radical yielding either an $S_t = 2$, 1, or 0 ground state, respectively. It is also conceivable that a charge distribution as in $[Fe^{II}(^3L^{\bullet})_2\{PR_3\}]^0$ prevails with an intrinsic spin at a *ferrous ion* of $S_{Fe} = 2$ (high spin), $S_{Fe} = 1$ (intermediate spin), or $S_{Fe} = 0$ (low spin) yielding the ground-state $S_t = 1$, 0, and 0, respectively.

In a preceding paper,[14] we have solved this problem for the electron-transfer series of some *dinuclear* species, as in eq 2, and shown that the redox steps are ligand centered and that, in each case, the ferric ions possess an intermediate

$$\underset{S_t = 0}{[Fe^{III}{}_2(^3L)_4]^{2-}} \underset{-e}{\overset{+e}{\rightleftharpoons}} \underset{S_t = {}^1/_2}{[Fe^{III}{}_2(^1L^{\bullet})(^1L)_3]^{1-}} \underset{-e}{\overset{+e}{\rightleftharpoons}} \underset{S_t = 0}{[Fe^{III}{}_2(^1L^{\bullet})_2(^1L)_2]^{0}} \qquad (2)$$

spin $S_{Fe} = {}^3/_2$. For this purpose, we had prepared[14] the new ligand 1,2-di(4-*tert*-butylphenyl)-1,2-ethylenedithiol, $H_2(^1L)$.

Scheme 1 shows the dithiolene ligands used in the present study, their abbreviations and their respective oxidation levels as either closed-shell dianions or π-radical monoanions. In addition, the new iron complexes synthesized are shown with their labels and spin states.

It is clearly established from crystallography[15−17] on square planar bis(dithiolene)metal complexes $[M^{II}(L)_2]^{2-}$ and $[M^{II}(L^{\bullet})_2]^0$ (M = Ni, Pd, Pt) that for a given dithiolene ligand the average C−S distances are significantly *longer* in the closed-shell dianions than in the corresponding π-radical monoanions (Δ(C−S) ≈ 0.05 Å).[13] Similarly, the olefinic C−C bond is *shorter* in the dianions than in the monoanions (Δ(C−C) ≈ 0.04 Å). In general, these two structural parameters allow the identification of the presence of two dianions *or* two monoanions in $[Fe(L)_2X]^n$ complexes. It is not possible to identify unambiguously the charge distribution when one dianion and one monoanion are present where the oxidation levels are delocalized as in $[Fe(L^{\bullet})(L)X]^n \leftrightarrow [Fe(L)(L^{\bullet})X]^n$.

Experimental Section

The dinuclear starting materials $[Fe^{III}{}_2(^1L^{\bullet})_2(^1L)_2$ and $[Fe^{III}{}_2(^3L^{\bullet})_2(^3L)_2]$ have been prepared as described previously.[4,14]

(7) Birchall, T.; Greenwood, N. N. *J. Chem. Soc. A* **1969**, 286.
(8) Dance, I. G.; Miller, T. R. *Inorg. Chem.* **1974**, *13*, 525.
(9) Epstein, E. F.; Bernal, I. *Inorg. Chim. Acta* **1977**, *25*, 145.
(10) Miyamae, H.; Sato, S.; Saito, Y.; Sakai, K.; Fukuyama, M. *Acta Crystallogr.* **1977**, *B33*, 3942.
(11) Fettouhi, M.; Morsy, M.; Waheed, A.; Golhen, S.; Ouahab, L.; Sutter, J.-P.; Kahn, O.; Menendez, N.; Varret, F. *Inorg. Chem.* **1999**, *38*, 4910.
(12) Sutter, J.-P.; Fettouhi, M.; Li, L.; Michaut, C.; Ouahab, L.; Kahn, O. *Angew. Chem., Int. Ed. Engl.* **1996**, *35*, 2113.
(13) *Dithiolene Chemistry*; Stiefel, E. I., Ed.; Progress in Inorganic Chemistry 52; Wiley, New York, 2004; pp 1−681.
(14) Patra, A. K.; Bill, E.; Weyhermüller, T.; Stobie, K.; Bell, Z.; Ward, M. D.; McCleverty, J. A.; Wieghardt, K. *Inorg. Chem.* submitted.
(15) Lim, B. S.; Fomitchev, D. V.; Holm, R. H. *Inorg. Chem.* **2001**, *40*, 4257.
(16) Dessy, G.; Fores, V.; Bellitto, C.; Flamini, A. *Cryst. Struct. Commun.* **1982**, *11*, 1743.
(17) (a) Sartain, D.; Truter, M. R. *J. Chem. Soc. A* **1967**, 1264. (b) Megnamisi-Belombe, M.; Nuber, B. *Bull. Chem. Soc. Jpn.* **1989**, *62*, 4092.

[N(*n*-Bu)$_4$][Fe^{II}(L$^{\bullet}$)$_2$(CN)]·1.5 toluene (1). A toluene solution (10 mL) of [N(*n*-Bu)$_4$]CN (0.038 g, 0.14 mmol) was added dropwise with vigorous stirring to a toluene solution (20 mL) of the dinuclear complex [Fe$^{III}_2$(L$^{\bullet}$)$_2$(L)$_2$] (0.10 g, 0.065 mmol) at 20 °C. An immediate color change from deep blue to dark green was observed. After the mixture was stirred for 2 h at 20 °C, the volume of the solution was reduced by evaporation under reduced pressure to 5 mL, and dry *n*-hexane (15 mL) was added. The solution was allowed to stand at 4 °C for 12 h; after which, dark green block-shaped crystals were filtered off, washed with *n*-hexane (10 mL), and dried. Yield: 0.065 g (76%). Electrospray mass spectrum (CH_2Cl_2, *m*/*z*): negative ion mode 790.3; calcd for [Fe(L)$_2$(CN)]$^-$ 790.0; positive ion mode 242, {N(*n*-Bu)$_4$}$^+$ 242. IR(KBr, cm^{-1}): ν_{CN} 2087. Anal. Calcd for $C_{61}H_{88}S_8N_2Fe$: C, 63.07; H, 7.64; S, 22.06; N, 2.41. Found: C, 63.0; H, 7.7; S, 22.0; N, 2.4.

The corresponding tetraethylammonium salt was prepared as described above by using an acetonitrile solution (2 mL) of [N(Et)$_4$]-CN (0.05 g; 0.32 mmol). Dark green single crystals of [N(Et)$_4$]-[Fe^{II}(L$^{\bullet}$)$_2$(CN)]·3 toluene (**1′**) of X-ray quality were slowly grown from a toluene solution of the tetraethylammonium salt.

[Fe^{III}(L$^{\bullet}$)$_2$(CN)] (1^{ox}). Method A. A toluene solution (10 mL) of [N(*n*-Bu)$_4$]CN (0.038 g, 0.14 mmol) was added dropwise to a stirred solution of [Fe$^{III}_2$(L$^{\bullet}$)$_2$(L)$_2$] (0.10 g, 0.065 mmol) in toluene (15 mL). The blue solution changed to dark green. After the mixture was stirred for 10 min at 20 °C, the toluene solution (5 mL) of ferrocenium hexaflurophosphate (0.052, 0.16 mmol) was added, producing a color change from green to blue. The solvent was completely removed by evaporation under reduced pressure, and the crude solid was washed successively with methanol (30 mL) and then acetonitrile (20 mL). Yield: 0.03 g (27%). IR (KBr, cm^{-1}): ν_{CN} 2139. Anal. Calcd for $C_{45}H_{52}S_4NFe$: C, 68.33; H, 6.63; N, 1.77. Found: C, 68.2; H, 6.6; N, 1.7.

Method B. A toluene solution (10 mL) of [N(*n*-Bu)$_4$]CN (0.038 g, 0.14 mmol) was added dropwise to a stirred solution of [Fe$^{III}_2$(L$^{\bullet}$)$_2$(L)$_2$] (0.10 g, 0.065 mmol) in toluene (15 mL). After the mixture was stirred for 1 h at 20 °C in the presence of air, the solvent was removed by evaporation under reduced pressure. The green residue was redissolved in 20 mL of acetonitrile, and an CH_3CN solution (5 mL) of ferrocenium hexafluorophosphate (0.052 g, 0.16 mmol) was added with stirring. A blue solid precipitated, which was collected by filtration, washed with CH_3CN and then CH_3OH, and dried. Yield: 0.05 g (45%).

[Cp$_2$Co][N(*n*-Bu)$_4$][Fe^{II}(L$^{\bullet}$)(L)(CN)] (1^{red}). A toluene solution (10 mL) of [N(*n*-Bu)$_4$]CN (0.038 g, 0.14 mmol) was added dropwise to a stirred solution of [Fe$^{III}_2$(L$^{\bullet}$)$_2$(L)$_2$] (0.10 g, 0.065 mmol) in toluene (15 mL). After the mixture was stirred at ambient temperature for 30 min, a toluene solution (5 mL) of cobaltocene (Cp_2Co) (0.03 g, 0.16 mmol) was added. A green microcrystalline precipitate formed within minutes and was collected by filtration, washed with toluene (30 mL), and dried. Yield: 0.11 g (69%). Anal. Calcd for $C_{71}H_{98}S_4CoFeN$: C, 69.75; H, 8.08; S, 10.49; N, 2.29. Found: C, 69.8; H, 8.0; S, 10.4; N, 2.2. IR (KBr, cm^{-1}): ν_{CN} 2047/2094.

[Fe^{III}(L$^{\bullet}$)$_2$I] (2). A toluene solution (10 mL) of iodine (0.036 g, 0.14 mmol) was added dropwise with stirring a 20 °C to a toluene solution (20 mL) of [Fe$^{III}_2$(L$^{\bullet}$)$_2$(L)$_2$] (0.20 g, 0.13 mmol), producing a color change from deep blue to dark violet. The solution was concentrated by evaporation of the solvent under reduced pressure to ~5 mL. *n*-Hexane (30 mL) was added slowly, and the flask was kept at 4 °C for 12 h. Needle-shaped microcrystals precipitated, which were collected by filtration, washed with *n*-hexane, and dried. Yield: 0.13 g (56%). Anal. Calcd for $C_{44}H_{52}S_4IFe$: C, 59.25; H, 5.88; S, 14.38. Found: C, 59.2; H, 5.8; S, 14.3.

[Fe^{II}(L$^{\bullet}$)$_2${P(OCH$_3$)$_3$}] (3). A toluene solution (5 mL) of $P(OCH_3)_3$ (0.022 g, 0.18 mmol) was added dropwise to a stirred solution of [Fe$^{III}_2$(L$^{\bullet}$)$_2$(L)$_2$] (0.10 g, 0.065 mmol) in toluene (10 mL). After the now dark green solution was stirred for 30 min, 2-propanol was allowed to diffuse into the solution. Within 3 days, fine needle-shaped crystals precipitated and were collected by filtration, washed with 2-propanol, and dried. Yield: 0.07 g (60%). Anal. Calcd for $C_{47}H_{61}S_4PO_3Fe$: C, 63.49; H, 6.92; S, 14.43. Found: C, 63.6; H, 6.8; S, 14.3.

[Fe^{II}(L$^{\bullet}$)$_2${P(OC$_6$H$_5$)$_3$}] (4). Excess triphenyl phosphite (0.5 mL) was added to a black suspension of [Fe$^{III}_2$(L$^{\bullet}$)$_2$(L)$_2$] (0.10 g, 0.09 mmol) in CH_2Cl_2 (15 mL). The solution was stirred at 20 °C for 12 h. The solvent was then removed by evaporation to give a green oil. This was purified by column chromatography (silica gel, CH_2Cl_2/*n*-hexane (1:1, v/v)); the first green band corresponded to the desired product. Yield: 0.15 g (95%). Anal. Calcd for $C_{46}H_{35}O_3S_4PFe$: C, 64.19; H, 4.09. Found: 64.03; H, 4.0. FABMS (*m*/*z*): 850 (M$^+$), 757 ({M − OPh}), 540 ({M − P(OPh)$_3$}$^+$).

X-ray Crystallographic Data Collection and Refinement of the Structures. A green single crystal of **1**·1.5 toluene and a specimen of **4** were coated with perfluoropolyether, picked up with a glass fiber, and immediately mounted in the nitrogen cold stream of the diffractometers to prevent loss of solvent. A Nonius Kappa-CCD diffractometer equipped with a Mo-target rotating-anode X-ray source and a graphite monochromator (Mo Kα, $\lambda = 0.71073$ Å) was used for **1**, and a sealed-tube source was used for **4**. Final cell constants were obtained from least-squares fits of all measured reflections. The intensity data of **4** were corrected for absorption using the intensities of redundant reflections. The structures were readily solved by Patterson methods and subsequent difference Fourier techniques. The Siemens SHELXTL[18] software package was used for solution and artwork of the structure, and SHELXL97[19] was used for the refinement. All non-hydrogen atoms were refined anisotropically. Hydrogen atoms were placed at calculated positions and refined as riding atoms with isotropic displacement parameters. Crystallographic data of the compounds are listed in Table 1.

Disorder in two out of three toluene solvent molecules was found in **1**. A restrained split atom model with occupation factors of about 2:1 was refined for the first (C501−C507 and C511−C517). The methyl group in a second toluene was split on two position in a 70:30 ratio (C607 and C617). Two tertiary butyl groups in one of the two crystallographically independent complex anions, attached to C(6) and C(42), were disordered. Split positions were refined with occupation ratios of about 75:25 and 58:42, respectively. A tetraethylammonium cation had also to be split on two positions. The occupation ratio refined to about 70:30. The geometries of the split models were restrained using SAME and SADI instructions of SHELXL97 (171 restraints).

Physical Measurements. The equipment used for IR, UV−vis, EPR, and Mössbauer spectroscopies has been described in refs 20−23. The temperature-dependent magnetic susceptibilities of solid samples of the complexes were measured by using a SQUID

(18) *SHELXTL*, version 5; Siemens Analytical X-ray Instruments Inc.: Madison, WI, 1994.
(19) Sheldrick, G. M. *SHELXL97*; Universität Göttingen: Göttingen, Germany, 1997.
(20) (a) Chun, H.; Bill, E.; Weyhermüller, T.; Wieghardt, K. *Inorg. Chem.* **2003**, *42*, 5612. (b) Chun, H.; Weyhermüller, T.; Bill, E.; Wieghardt, K. *Angew. Chem., Int. Ed.* **2001**, *40*, 2489.
(21) Chłopek, K.; Bill, E.; Weyhermüller, T.; Wieghardt, K. *Inorg. Chem.* **2005**, *44*, 7087.

Table 1. Crystallographic Data for **1**·1.5Toluene and **4**

	1·1.5toluene	**4**
chemical formula	$C_{63.5}H_{84}FeN_2S_4$	$C_{46}H_{35}FeO_3PS_4$
fw	1059.42	850.80
space group	$P2_1/c$ (No. 14)	$P\bar{1}$ (No. 2)
a (Å)	20.634(2)	11.078(2)
b (Å)	15.9296(12)	13.382(4)
c (Å)	36.048(3)	14.845(4)
α (deg)	90	105.02(3)
β (deg)	90.508(5)	91.50(2)
γ (deg)	90	107.80(2)
V (Å^3)	11848.2(18)	2010.5(8)
Z	8	2
T (K)	100(2)	173(2)
ρ_{calcd} (g cm^{-3})	1.188	1.405
reflns collected/$2\Theta_{max}$	34 339/45.00	21 276/55.08
unique reflns/$I > 2\sigma(I)$	13 544/10 492	9116/5201
no. of params/restraints	1371/171	496/0
λ (Å)/μ(Kα) (cm^{-1})	0.71073/4.35	0.71073/6.64
R1[a]/GOF[b]	0.0865/1.173	0.0459/0.988
wR2[c] ($I > 2\sigma(I)$)	0.1479	0.0866
residual density (e Å^{-3})	+0.44/ −0.40	+0.51/ −0.39

[a] Observation criterion: $I > 2\sigma(I)$. R1 = $\sum||F_o| - |F_c||/\sum|F_o|$. [b] GOF = $[\sum[w(F_o^2 - F_c^2)^2]/(n-p)]^{1/2}$. [c] wR2 = $[\sum[w(F_o^2 - F_c^2)^2]/\sum[w(F_o^2)^2]]^{1/2}$, where $w = 1/\sigma^2(F_o^2) + (aP)^2 + bP$, $P = (F_o^2 + 2F_c^2)/3$.

magnetometer (Quantum Design) at 1.0 T (4.2−300 K). Corrections for underlying diamagnetism were made using tabulated Pascal's constants. Cyclic voltammograms and coulometric experiments were performed with an EG&G potentiostat/galvanostat in CH_2Cl_2 solutions (0.10 M $[N(n\text{-}Bu)_4]PF_6$) at a glassy carbon working electrode. Ferrocene was used as internal standard; all redox potentials are given versus the ferrocenium/ferrocene (Fc^+/Fc) couple.

Calculations. All DFT calculations were performed with the ORCA program package.[24] The geometry optimizations of the complexes were carried out at the B3LYP[25−27] level of DFT. The all-electron Gaussian basis sets were those reported by the Ahlrichs group.[28,29] For neutral $[Fe(L)_2(CN)]$, triple-ζ quality basis sets TZV(P) with one set of polarization functions on the iron and on the atoms directly coordinated to the metal center were used.[29] The carbon, nitrogen, and hydrogen atoms were described by slightly smaller polarized split-valence SV(P) basis sets which are double-ζ quality in the valence region and contain a polarizing set of d-functions on the non-hydrogen atoms.[28] For the monoanion $[Fe(L)_2(CN)]^{1-}$, the TZV(P) basis set of all non-hydrogen atoms was augmented by one diffuse function for every valence shell, choosing an exponent equal to one-third of the smallest exponent in the respective shell. The auxiliary basis sets for all complexes used to expand the electron density in the calculations were chosen to match the orbital basis.[30] The SCF calculations were tightly converged (1×10^{-8} E_h in energy, 1×10^{-7} E_h in the density change, and 1×10^{-7} in maximum element of the DIIS error vector). The geometry search was carried out in redundant internal coordinates without imposing symmetry constraints. The geometries were considered converged after the energy change was les than 5×10^{-6} E_h, the gradient norm and maximum gradient element were smaller than 1×10^{-4} E_h/bohr and 3×10^{-4} E_h/bohr, respectively, and the root-mean square and maximum displacements of all atoms were smaller than 2×10^{-3} and 4×10^{-3} bohr, respectively. Corresponding[31] canonical orbitals and density plots were obtained using the program Molekel.[32]

The present calculations were performed on truncated models where the four 4-*tert*-butylphenyl groups of the basal ligands were substituted by methyl groups. Nonrelativistic single-point calculations on the optimized geometries of the iron complexes with the B3LYP functional were carried out to obtain Mössbauer spectral parameters (isomer shifts and quadrupole splittings). These calculations employed the CP(PPP) basis set[33] for iron and the TZV(P) basis sets for the N and C atoms. The SV(P) basis sets were used for the remaining atoms. The Mössbauer isomer shifts were calculated from the computed electron densities at the iron centers as previously described.[34]

Synthesis and Characterization of Complexes

As in the original syntheses of mononuclear bis(dithiolene)iron complexes by Holm, Balch, and McCleverty et al.,[1−5] the dinuclear complex $[Fe^{III}_2(^1L^\bullet)_2(^1L)_2]^0$ [14] was treated with $[N(n\text{-}Bu)_4]CN$ (1:2) in toluene solution to yield dark green crystals of $[N(n\text{-}Bu)_4][Fe^{II}(^1L^\bullet)_2(CN)]$ (**1**), eq 1. When $[NEt_4]CN$ was used, the salt $[NEt_4][Fe^{II}(^1L^\bullet)_2(CN)]$·1.5 toluene (**1′**) was obtained as larger crystals suitable for X-ray crystallography. Complex **1** and **1′** are diamagnetic ($S_t = 0$)

$$[Fe^{III}_2(^1L^\bullet)_2(^1L)_2]^0 + 2\ CN^- \xrightarrow{\text{toluene}} 2\ [Fe^{II}(^1L^\bullet)_2(CN)]^- \quad (1)$$

as shown by applied field Mössbauer spectroscopy (see below).

The monoanion in **1** can be one-electron oxidized in toluene solution via the addition of 1 equiv of ferrocenium hexaflurophosphate, eq 2, affording a blue microcrystalline precipitate of $[Fe^{III}(^1L^\bullet)_2(CN)]^0$ (**1**^{ox}). Complex **1**^{ox} is paramagnetic and possesses an $S_t = {}^1/_2$ ground state (see below).

$$\underset{\mathbf{1}}{[Fe^{II}(^1L^\bullet)_2(CN)]^-} + [Cp_2Fe]^+ \rightarrow \underset{\mathbf{1}^{ox}}{[Fe^{III}(^1L^\bullet)_2(CN)^0]} + [Cp_2Fe]^0 \quad (2)$$

The one-electron reduced form of **1** is also chemically accessible by using 1 equiv of cobaltocene as reductant, eq 3. Thus, green microcrystals of $[Cp_2Co][N(n\text{-}Bu)_4][Fe^{II}(^1L^\bullet)(^1L)(CN)]$ (**1**^{red}) have been obtained. Complex **1**^{red} is also paramagnetic with an $S_t = {}^1/_2$ ground state. We note that the

(22) (a) Ghosh, P.; Bill, E.; Weyhermüller, T.; Wieghardt, K. *J. Am. Chem. Soc.* **2003**, *125*, 3967. (b) Ghosh, P.; Begum, A.; Bill, E.; Weyhermüller, T.; Wieghardt, K. *Inorg. Chem.* **2003**, *42*, 3208.
(23) Ray, K.; Bill, E.; Weyhermüller, T.; Wieghardt, K. *J. Am. Chem. Soc.* **2005**, *127*, 5641.
(24) Neese, F. *ORCA, An Ab Initio, Density Functional and Semiempirical Electronic Structure Program Package*, version 2.4, revision 36; Max-Planck-Institut für Bioanorganische Chemie: Mülheim/Ruhr, Germany, 2005.
(25) Becke, A. D. *J. Chem. Phys.* **1986**, *84*, 4524.
(26) Becke, A. D. *J. Chem. Phys.* **1993**, *98*, 5648. (b) Lee, C. T.; Yang, W. T.; Parr, R. G. *Phys. Rev. B* **1988**, *37*, 785.
(27) Stephens, P. J.; Devlin, F. J.; Chabalowski, C. F.; Frisch, M. J. *J. Phys. Chem.* **1994**, *98*, 11623.
(28) Schäfer, A.; Horn, H.; Ahlrichs, R. *J. Chem. Phys.* **1992**, *97*, 2571.
(29) Schäfer, A.; Huber, C.; Ahlrichs, R. *J. Chem. Phys.* **1994**, *100*, 5829.
(30) (a) Eichkorn, K.; Weigend, F.; Treutler, O.; Ahlrichs, R. *Theor. Chem. Acc.* **1997**, *97*, 119. (b) Eichkorn, K.; Treutler, O.; Ohm, H.; Haser, M.; Ahlrichs, R. *Chem. Phys. Lett.* **1995**, *242*, 652. (c) Eichkorn, K.; Treutler, O.; Ohm, H.; Haser, M.; Ahlrichs, R. *Chem. Phys. Lett.* **1995**, *240*, 283.
(31) Neese, F. *J. Phys. Chem. Solids* **2004**, *65*, 781.
(32) Molekel, Ed. *Molekel, Advanced Interactive 3D-Graphics for Molecular Sciences*; available at http://www.cscs.ch/molekel/.
(33) Neese, F. *Inorg. Chim. Acta* **2002**, *337*, 181.
(34) Sinnecker, S.; Slep, L. D.; Bill, E.; Neese, F. *Inorg. Chem.* **2005**, *44*, 2245.

$$[Fe^{II}(^1L^{\bullet})_2(CN)]^{1-} + Cp_2Co \rightarrow \underset{\mathbf{1}}{} \quad [Fe^{II}(^1L^{\bullet})(^1L)(CN)]^{2-} + [Cp_2Co]^{+} \quad (3)$$
$$\mathbf{1^{red}}$$

corresponding complex $[N(n\text{-}Bu)_4]_2[Fe(mnt)_2(CN)]$ ($S_t = {}^1/_2$) has been described by McCleverty et al.[2]

In the infrared spectra of solid **1**, $\mathbf{1^{ox}}$, and $\mathbf{1^{red}}$ (KBr disks), the ν(C≡N) stretching mode is observed at 2092, 2138, and 2047 cm^{-1}, respectively. This mode is primarily sensitive to the overall charge of the mononuclear species; it is observed at the highest energy in the neutral species $\mathbf{1^{ox}}$ and at the lowest in the dianion $\mathbf{1^{red}}$. It is also of interest that all three species display a band at ~1154 cm^{-1} which has been assigned in the previous paper on dinuclear species[14] as a ν(C═Ṡ) stretching mode. This fact indicates that in all three species at least one $(^1L^{\bullet})^{1-}$ π-radical ligand is present.

The dinuclear neutral complex $[Fe^{III}_2(^1L^{\bullet})_2(^1L)_2]$ was oxidized in toluene solution by 1 equiv of elemental iodine, eq 4, yielding dark bluish violet microcrystals of $[Fe^{III}(^1L^{\bullet})_2I]$ (**2**). This complex possesses an $S_t = {}^1/_2$ ground state.

$$[Fe^{III}_2(^1L^{\bullet})_2(^1L)_2] + I_2 \rightarrow 2\,[Fe^{III}(^1L^{\bullet})_2I] \quad (4)$$

Finally, the reaction of $[Fe^{III}_2(^1L^{\bullet})_2(^1L)_2]$ with 2.5 equiv of $P(OCH_3)_3$ in toluene yielded dark green crystals of $[Fe^{II}(^1L^{\bullet})_2\{P(OCH_3)_3\}]$ (**3**), which are diamagnetic ($S_t = 0$). Similarly, the reaction of $[Fe^{III}_2(^3L^{\bullet})_2(^3L)_2]$ with $P(OPh)_3$ afforded dark green, crystalline, diamagnetic $[Fe^{II}(^3L^{\bullet})_2\{P(OPh)_3\}]$ (**4**). This compound has been prepared previously.[3] It is noted that $[Fe^{II}(^3L^{\bullet})_2\{P(OCH_3)_3\}]$ has been previously synthesized[2,3] and structurally characterized by room-temperature X-ray crystallography.[10]

Electro- and Spectroelectrochemistry. Cyclic voltammograms (cv) of **1**, **3**, and **4** have been recorded in CH_2Cl_2 solutions containing 0.10 M $[N(n\text{-}Bu)_4]PF_6$ as the supporting electrolyte using a glassy carbon working electrode. Ferrocene was used as internal standard, and all potentials are referenced versus the ferrocenium/ferrocene couple (Fc^+/Fc).

Figure 1 shows the cv of **1** which displays two reversible one-electron transfer waves. Coulometric measurements at appropriately fixed potentials show that the first reversible wave at $E^1_{1/2} = -0.16$ V corresponds to a one-electron oxidation yielding $\mathbf{1^{ox}}$, whereas the second wave at $E^2_{1/2} = -1.16$ corresponds to a one-electron reduction affording $\mathbf{1^{red}}$. Figure 2 shows the spectral changes observed during oxidation, **1** → $\mathbf{1^{ox}}$ (top), and reduction, **1** → $\mathbf{1^{red}}$ (bottom). The electronic spectra of **1**, $\mathbf{1^{ox}}$, and $\mathbf{1^{red}}$ are summarized in Table 2.

The cvs of **3** and **4** are very similar, and only that for **3** will be presented in Figure 3. Both compounds exhibit a reversible one-electron oxidation wave at $E^1_{1/2} = 0.25$ V for **3** and at +0.38 V for **4**, yielding the monocationic species $\mathbf{3^{ox}}$ and $\mathbf{4^{ox}}$, respectively. When potentials more negative than 0.0 V are scanned, a complicated electrochemical response is observed at moderate scan rates (~100 mV s^{-1}). On the other hand, increasing the scan rate to 34 V s^{-1} leads to a simplified signal wave at $E^2_{1/2} = -0.96$ V, which corresponds to a single, reversible one-electron reduction affording $\mathbf{3^{red}}$ and $\mathbf{4^{red}}$, respectively. The additional waves in the top cv of Figure 3 at negative potentials are the result of dimer formation, $[Fe_2(^1L)_4]^n$ and $[Fe_2(^3L)_4]^n$, as described in ref 14.

Thus, **3** and **4** dissociate in solution upon reduction and dimerize as shown in Scheme 2. This dissociation of

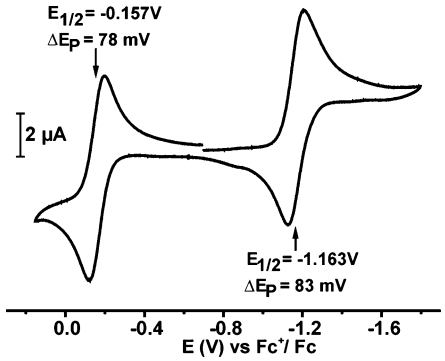

Figure 1. Cyclic voltammogram of **1** in CH_2Cl_2 (0.10 M $[N(n\text{-}Bu)_4]PF_6$) at 20 °C (glassy carbon working electrode, scan rate of 100 mV s^{-1}, ferrocene internal standard).

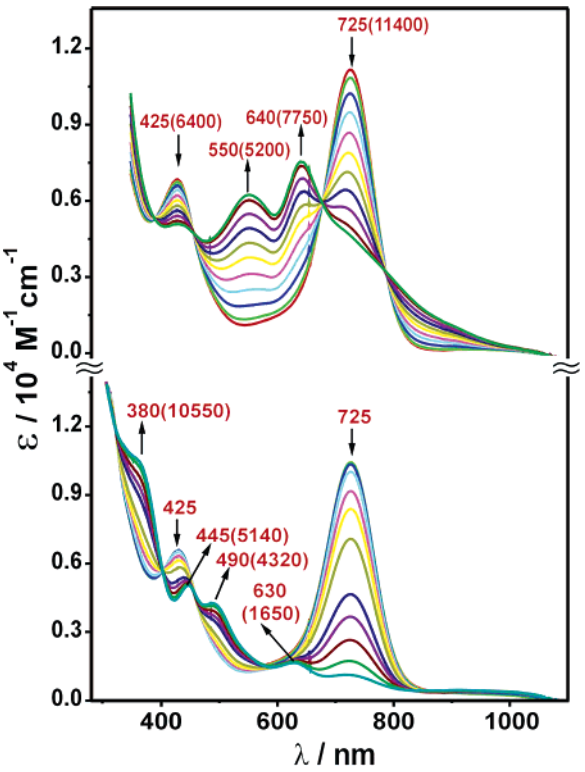

Figure 2. (top) Electronic spectral changes observed during the oxidation of **1** yielding $\mathbf{1^{ox}}$. (bottom) Changes during the reduction of **1** to $\mathbf{1^{red}}$ in CH_2Cl_2 solution. Wavelengths are given in nm, and the molar extinction coefficients, ϵ (in brackets), are given in M^{-1} cm^{-1}.

Table 2. Electronic Spectra of Complexes in CH_2Cl_2 Solution

	λ_{max}, nm (ϵ, $\times 10^4$ M^{-1} cm^{-1})
1	425 (0.5), 723 (1.1)
$\mathbf{1^{ox}}$	425 (0.5), 550 (0.6), 640 (0.8)
$\mathbf{1^{red}}$	380 (1.0), 445 (0.5), 490 (0.4), 630 (0.16)
2	485 (1.1), 555 (1.2), 665 (1.6), 820 (0.25)
3	375 (1.4), 460 sh (0.4), 702 (2.4)
$\mathbf{3^{ox}}$	268 (4.0), 306 (3.3), 427 (0.8), 515 (0.8), 675 (2.2), 920 (0.4)
$\mathbf{3^{red}}$	262 (3.7), 366 (1.4), 488 (0.5), 697 (0.5)
4	270 (3.9), 316 sh, 364 (1.0), 453 (0.5), 687 (1.8)
$\mathbf{4^{ox}}$	266 (3.1), 311 sh, 523 sh, 673 (1.5), 896 sh

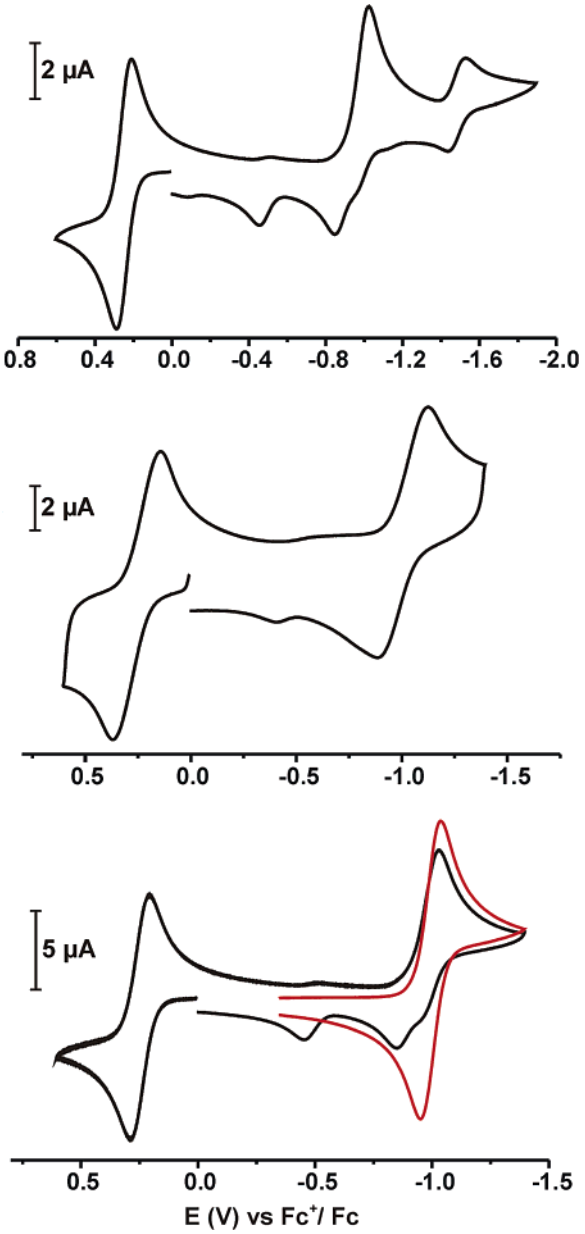

Figure 3. Cyclic voltammograms of **3** in CH_2Cl_2 (0.10 M $[N(n\text{-}Bu)_4]PF_6$) at 20 °C: (top) scan rate of 100 mV s^{-1}, (middle) scan rate of 34 V s^{-1}, (bottom) scan rate of 100 mV s^{-1}, and (in red) after the addition of excess $P(OCH_3)_3$.

Scheme 2. Redox Scheme for the Reduction of **3**.

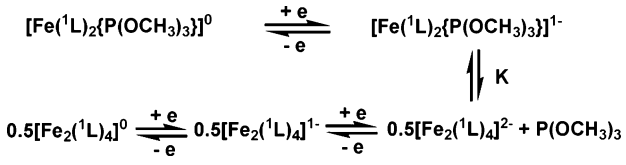

$[Fe(^1L)_2\{P(OCH_3)_3\}]^-$ can be suppressed by the addition of excess $P(OCH_3)_3$ (cv, no. 3 in Figure 3), upon which a fully reversible reduction wave is observed at $E^2_{1/2} = -0.95$ V for the $[Fe(^1L)_2\{P(OCH_3)_3\}]^{0/1-}$ couple.

Figure 4 shows the electronic spectra of **3** and $\mathbf{3}^{ox}$ which are remarkably similar to those shown in Figure 2 for **1** and $\mathbf{1}^{ox}$; this strongly suggests that neutral $\mathbf{1}^{ox}$ and cationic $\mathbf{3}^{ox}$ or $\mathbf{4}^{ox}$ have the same electronic structures. This also holds true for monoanionic **1** and neutral **3** or **4**. The spectra of

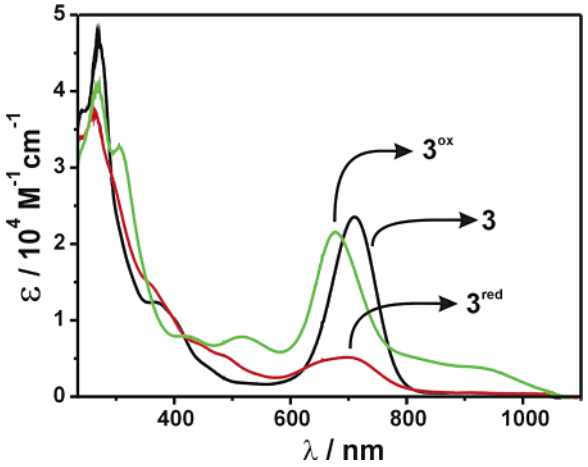

Figure 4. Electronic spectra of **3** (black), $\mathbf{3}^{ox}$ (green), and $\mathbf{3}^{red}$ (red) in CH_2Cl_2.

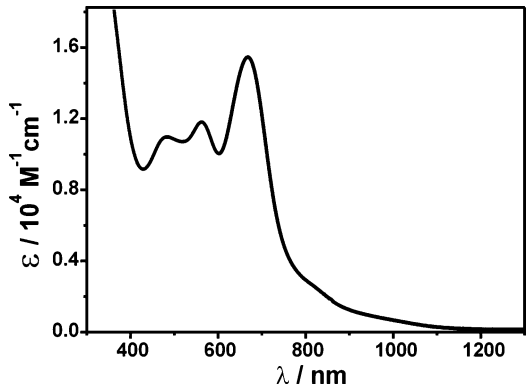

Figure 5. Electronic spectrum of **2** in CH_2Cl_2 solution at 20 °C.

$\mathbf{3}^{red}$ and $\mathbf{4}^{red}$ (monoanions) have not been recorded because of their lability in solution. The spectrum of **2** is shown in Figure 5; it resembles those of $\mathbf{1}^{ox}$ and $\mathbf{3}^{ox}$, $\mathbf{4}^{ox}$. The presence of a very intense ($\epsilon > 1.0 \times 10^4$ M^{-1} cm^{-1}) absorption maximum at >600 nm is indicative of the presence of two ligand π-radical anions, $(^1L^{\bullet})^{1-}$ or $(^3L^{\bullet})^{1-}$, as in the chromophores $Fe^{II}(L^{\bullet})_2X$ or $Fe^{III}(L^{\bullet})_2X$; it is essentially a ligand-to-ligand charge-transfer band (LLCT).

Crystal Structures. The crystal structures of **1** and **4** have been determined at 100 K. Crystallographic details are given in Table 1, and selected bond distances are listed in Table 3.

Crystals of **1** consist of well-separated tetraethylammonium cations and mononuclear five-coordinate monoanions $[Fe^{II}(^1L^{\bullet})_2(CN)]^{1-}$, shown in Figure 6 (top). The cyanide ligand occupies the apical position of a square-based pyramidal FeS_4C coordination polyhedron. The two bidentate dithiolato ligands are bound in the equatorial positions. The iron ion is, on average, 0.25 Å above the best plane of the four sulfur atoms of each of the two crystallographically independent monoanions in **1**.

It is important to note that the oxidation level of both equivalent disulfur ligand anions is best described as the π-radical anion $(^1L^{\bullet})^{1-}$. The average C−S distance is rather short at 1.72 Å, and the average olefinic C−C bond at 1.38 Å is longer than in the closed-shell dianionic form (~1.36 Å). These assignments render the central iron ion divalent,

Table 3. Selected Bond Distances (Å)[a]

	Complex **1**		
Fe(1)−S(1)	2.157(2)	Fe(1)−S(31)	2.143(2)
Fe(1)−S(2)	2.161(2)	Fe(1)−S(32)	2.163(2)
S(1)−C(1)	1.735(6)	S(31)−C(31)	1.713(6)
S(2)−C(2)	1.717(7)	S(32)−C(32)	1.717(7)
C(1)−C(2)	1.379(9)	C(31)−C(32)	1.383(9)
Fe(1)−C(55)	1.887(7)		
C(55)−N(56)	1.145(8)		
	Complex **4**		
Fe(1)−S(2)	2.166(1)	Fe(1)−S(4)	2.153(1)
Fe(1)−S(3)	2.150(1)	Fe(1)−S(5)	2.161(1)
S(2)−C(20)	1.699(3)	S(4)−C(40)	1.711(3)
S(3)−C(30)	1.700(3)	S(5)−C(50)	1.709(3)
C(20)−C(30)	1.399(4)	C(40)−C(50)	1.392(4)
Fe(1)−P(1)	2.132(1)		

[a] For **1**, data are given only for one crystallographically independent monoanion.

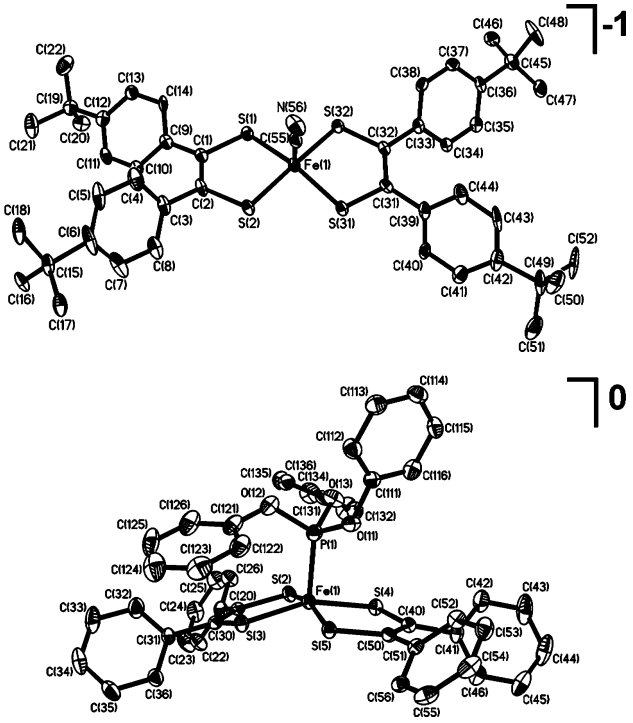

Figure 6. Structure of one of the monoanions $[Fe^{II}(^1L^{\bullet})_2(CN)]^{1-}$ in crystals of **1** (top) and of the neutral complex in crystals of **4** (bottom).

and the electronic structure of the monoanion is best denoted as $[Fe^{II}(^1L^{\bullet})_2(CN)]^{1-}$. In fact, the same ligand dimensions have been determined for the square planar, diamagnetic, neutral complexes $[M^{II}(^1L^{\bullet})_2]$ (M = Ni, Pd, Pt).[15−17]

The structure of the neutral molecule in crystals of **4** is displayed in Figure 6 (bottom). Again the central iron ion is in a square-based pyramidal environment of two equatorial ethenedithiolato anions and an apical $P(OPh)_3$ ligand where the Fe ion is 0.36 Å above the S_4 plane. The dimensions of the two chelating disulfur ligands are within experimental error identical; the average short C−S bond distance of 1.705(3) Å and the longer olefinic C−C bond at 1.395 Å are again indicative of two π-radical monoanions $(^3L^{\bullet})^{1-}$, rendering the oxidation state of the iron ion divalent.

We note that the room-temperature crystal structure of isoelectronic $[Fe(^3L^{\bullet})_2\{P(OCH_3\}]$ has been reported in 1977:[10] the average C−S length is 1.717 Å and the average olefinic C−C bond at 1.397 Å is long. Similar results have been obtained[9] for $[Fe^{II}(S_2C_2\{CF_3\}_2)_2\{AsPh_3\}]^0$, where the authors did note the short average C−S distance at 1.702 Å. The olefinic C−C distance of 1.37 Å is in good agreement with a radical oxidation level of the monoanionic ligands.

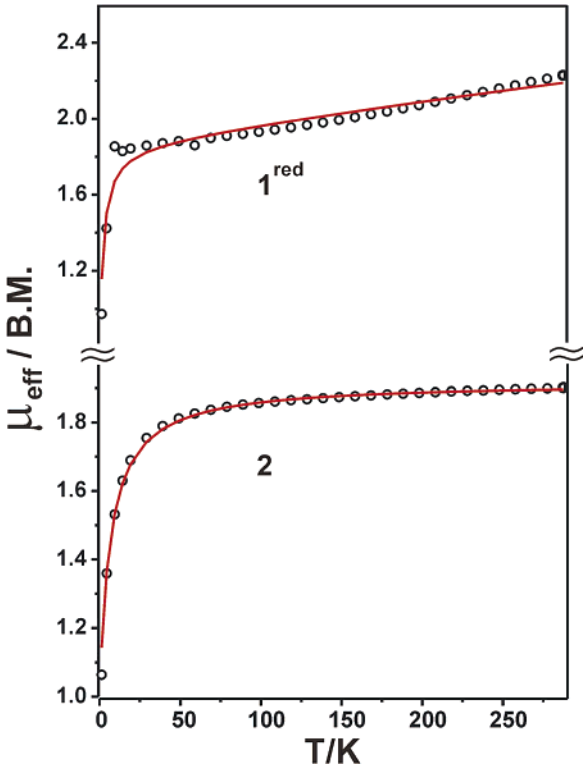

Figure 7. Temperature-dependence of the magnetic moment, μ_{eff} and μ_B, of $\mathbf{1}^{red}$ (top) and **2** (bottom). The solid lines represent best fits to models described in the text; open circles are the experimental data.

In the mononuclear complex $[Fe^{III}(mnt)_2(idzm)]^0$, where $idzm^+$ represents the cation 2(*p*-pyridyl)-4,4,5,5-tetramethylimidazolinium,[11] the average C−S distance of 1.743 Å is long, and the olefinic C−C bond is short at 1.353(5) Å, indicating the presence of two closed-shell $(mnt)^{2-}$ ligands with an intermediate spin ferric ion ($S_t = S_{Fe} = {}^3/_2$).

Magnetic Properties and EPR Spectroscopy. Temperature-dependent magnetic susceptibilities of complexes have been measured at an external magnetic field of 1.0 T (4−300 K). Complexes **1**, **3**, and **4** were found to be diamagnetic at room temperature; they possess an $S_t = 0$ ground state.

The μ_{eff} versus *T* plots for $\mathbf{1}^{red}$ (top) and **2** (bottom) are shown in Figure 7. The slight increase of μ_{eff} in the range 150−300 K for $\mathbf{1}^{red}$ was successfully modeled by using a coupling model between an intermediate spin ferrous ion ($S_{Fe} = 1$) and a ligand π radical, $(^1L^{\bullet})^{1-}$ ($H = -2JS_{Fe}S_{rad}$, $S_{Fe} = 1$, $S_{rad} = {}^1/_2$). An antiferromagnetic coupling constant of -228 cm^{-1}, temperature-independent paramagnetism, $\chi_{TIP} = 249 \times 10^{-6}$ cm^3 mol^{-1}, and a Weiss constant of $\theta = -9.4$ K yielded the fit shown in Figure 7 (top).

The bottom plot of Figure 7 shows the temperature dependence of the magnetic moment of **2**, which exhibits the spin-only value of a single unpaired electron in the range of 70−300 K (~1.8 μ_B). The fit required a paramagnetic

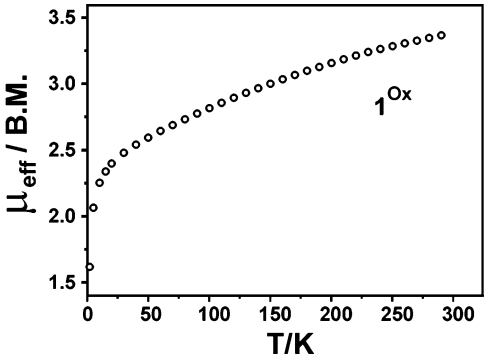

Figure 8. Temperature-dependence of the magnetic moment of the spin-crossover system of solid $\mathbf{1}^{ox}$. The data agree nicely with Mössbauer data shown in Figure 13.

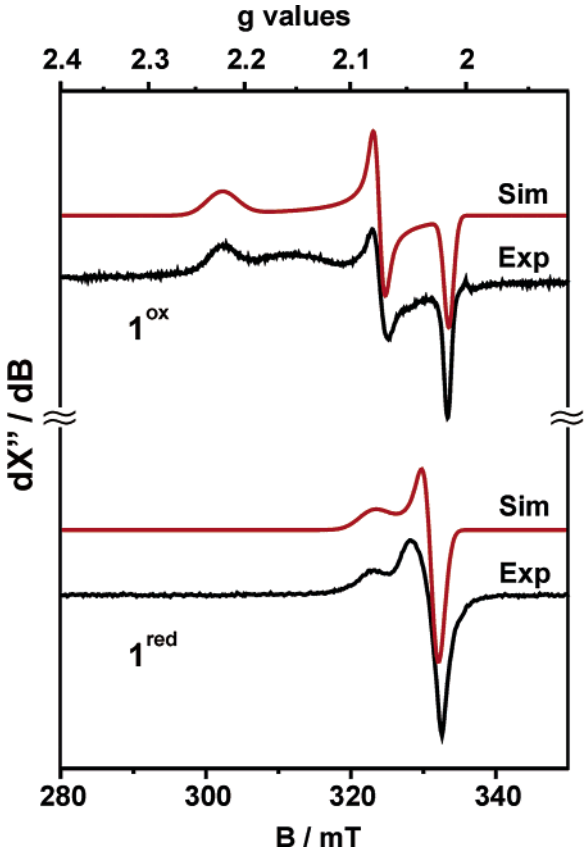

Figure 9. X-band EPR spectra of frozen CH_2Cl_2 solutions of $\mathbf{1}^{ox}$ (top) and electrochemically generated $\mathbf{1}^{red}$ (bottom) at 10 K. Conditions: frequency = 9.43 GHz, modulation = 10.0 G, power = 100 μW. For simulation parameters see text.

impurity of 2% ($S = {}^5/_2$), and for the low-temperature region, weak intermolecular, antiferromagnetic coupling was taken into account by a Weiss constant $\theta = -8.3$ K.

Figure 8 displays the μ_{eff} versus T plot for neutral $\mathbf{1}^{ox}$. The magnetic moment decreases monotonically from 3.3 μ_B at 300 K to 1.6 K at 2 K which indicates a gradual spin-crossover phenomenon in $\mathbf{1}^{ox}$ between an $S_t = {}^3/_2$ and an $S_t = {}^1/_2$ state. These data are in agreement with the Mössbauer data (see below).

The X-band EPR spectra of the $S_t = {}^1/_2$ complexes $\mathbf{1}^{ox}$ (top) and $\mathbf{1}^{red}$ (bottom) in frozen CH_2Cl_2 solution at 10 K are shown in Figure 9. The former displays a rhombic signal with pronounced g anisotropy, $g_x = 2.23$, $g_y = 2.08$, and $g_z = 2.02$, whereas the latter shows an axial signal of small g anisotropy, $g_z = 2.09$ and $g_{x,y} = 2.03$.

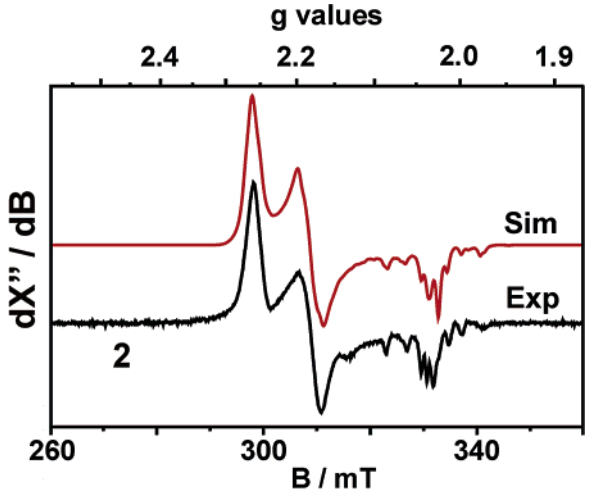

Figure 10. X-band EPR spectrum of **2** in frozen acetonitrile/toluene (1:1 v/v) at 10 K. Conditions: frequency = 9.43 GHz, modulation = 5.0 G, power = 2.52 μW. For simulation parameters see text.

As we will show below, the electronic structure of $\mathbf{1}^{ox}$ is best described as $[Fe^{III}(L^{\bullet})_2(CN)]$, where the intermediate spin ferric ion ($S_{Fe} = {}^3/_2$) is antiferromagnetically coupled to two ligand π radicals $({}^1L^{\bullet})^{1-}$, yielding the observed $S_t = {}^1/_2$ ground state. The unpaired electron resides then in a metal d orbital which is in agreement with the large g anisotropy. For $\mathbf{1}^{red}$, an electronic structure, as shown by the two resonance structures $[Fe^{II}({}^1L^{\bullet})({}^1L)(CN)]^{2-} \leftrightarrow [Fe^{II}({}^1L)({}^1L^{\bullet})(CN)]^{2-}$, is proposed.

If the intrinsic spin state at the Fe(II) ion is intermediate spin ($S_{Fe} = 1$), antiferromagnetic coupling to a ligand π radical would yield an $S_t = {}^1/_2$ ground state, but the unpaired electron would possess predominantly metal d character. In contrast, a low-spin ferrous ion ($S_{Fe} = 0$) in $\mathbf{1}^{red}$ would place the unpaired electron at the ligand π radical $({}^1L^{\bullet})^{1-}$. The observed small g anisotropy at $g \approx 2$ would be in excellent agreement with a sulfur-centered radical (e.g., for $[Au^{III}(L^{Bu})(L^{Bu\bullet})] \leftrightarrow [Au^{III}(L^{Bu\bullet})(L^{Bu})]$ ($S = {}^1/_2$) g values at 2.0690, 2.0320, and 1.911 have been reported).[35]

The X-band EPR spectrum of **2** in a frozen toluene/acetonitrile mixture (1:1 v/v) at 10 K is shown in Figure 10; it shows some very interesting and unusual features.

The rhombic signal, $g_x = 2.25905$, $g_y = 2.17969$, and $g_z = 2.02700$, shows the same g anisotropy as the spectrum of $\mathbf{1}^{ox}$, and therefore, the same electronic structure prevails in **2**: $[Fe^{III}({}^1L^{\bullet})_2I]$ where an intermediate spin ferric ion is antiferromagnetically coupled to two ligand π radicals $({}^1L^{\bullet})^{1-}$. The hyperfine structure at g_z is caused by hyperfine and quadrupole coupling to the coordinated iodide: $A_x = 7.46 \times 10^{-4}$, $A_y = 6.28 \times 10^{-4}$, $A_z = 24 \times 10^{-4}$ cm^{-1} and $P_x = 11.7 \times 10^{-4}$, $P_y = -13.19 \times 10^{-4}$, $P_z = 1.49 \times 10^{-4}$ cm^{-1}. The complexes shown in Figure 11 all display very similar EPR spectra regardless of the nature of the two ligand π radicals.[20−23]

(35) Ray, K.; Weyhermüller, T.; Goossens, A.; Craje, M. W. J.; Wieghardt, K. *Inorg. Chem.* **2003**, *42*, 4082.

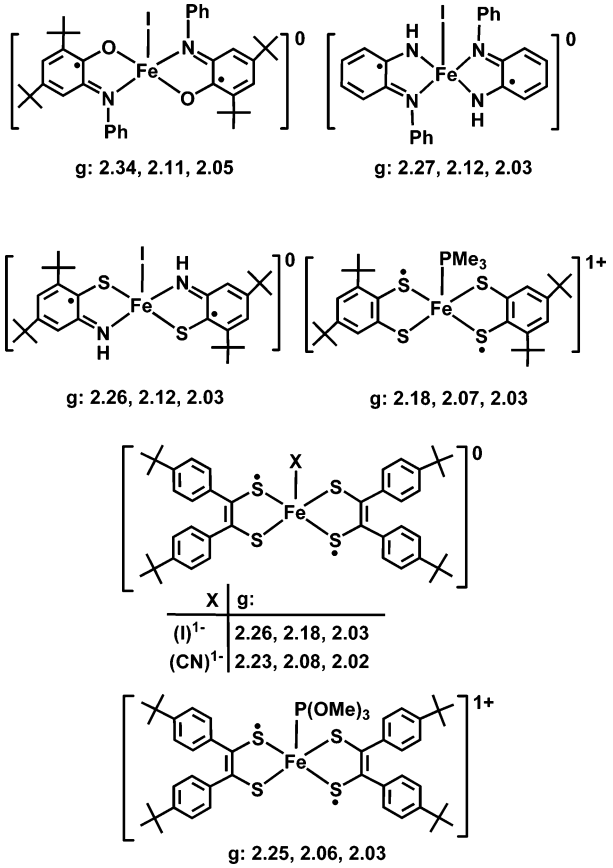

Figure 11. Structurally and EPR spectroscopically characterized five-coordinate complexes containing an intermediate-spin ferric ion ($S_{Fe} = {}^3/_2$) and two π-radical ligands ($S_t = {}^1/_2$). The numbers refer to the reported g_x, g_y, and g_z values from refs 20−23 for the first four complexes.

Figure 12 shows the X-band EPR spectra of the monocation **3**^{ox} (top) and of the monoanion **3**^{red} (bottom) in frozen CH_2Cl_2 solution (0.10 M [N(*n*-Bu)$_4$]PF$_6$) at 10 K. Both exhibit rhombic signals. The former also displays resolved ^{31}P hyperfine splitting. Thus, the spectrum of **3**^{ox} has been successfully simulated with $g_x = 2.25$, $g_y = 2.06$, $g_z = 2.03$; $A_{xx}(^{31}P) = 0$, $A_{yy}(^{31}P) = 35.2 \times 10^{-4}$, $A_{zz}(^{31}P) = 32.7 \times 10^{-4}$ cm^{-1}.

The electronic structure is $[Fe^{III}(^1L^{\bullet})_2\{P(OCH_3)_3\}]^+$ with an unpaired electron in an Fe d orbital. In contrast, the g anisotropy is significantly smaller in **3**^{red}: $g_x = 2.06$, $g_y = 2.02$, and $g_z = 2.01$ with no resolved ^{31}P coupling. The simulation shown in Figure 12 (bottom) invokes ^{31}P hyperfine coupling constants: $A_{xx}(^{31}P) = 10 \times 10^{-4}$, $A_{yy}(^{31}P) = 37 \times 10^{-4}$, and $A_{zz}(^{31}P) = -3.8 \times 10^{-4}$ cm^{-1}. The electronic structure of **3**^{red} may be described as $[Fe^{II}(^1L^{\bullet})(^1L)\{P(OCH_3)_3\}]^{1-} \leftrightarrow [Fe^{II}(^1L)(^1L^{\bullet})\{P(OCH_3)_3\}]^{1-}$, where the intrinsic spin state at Fe(II) is assumed to be $S_{Fe} = 1$, as in **1**^{red}.

Finally, we have also recorded the X-band EPR spectrum of **4**^{ox} ($S_t = {}^1/_2$) in frozen CH_2Cl_2 (0.10 M [N(*n*-Bu)$_4$]PF$_6$) at 25 K which is shown in Figure S1. A satisfactory simulation was obtained with g values (2.272, 2.073, 2.019) and $A(^{31}P) = (13.3, 22.1, 20.0) \times 10^{-4}$ cm^{-1}. The large g anisotropy and the ^{31}P hyperfine splitting are characteristic for an $[Fe^{III}(^3L^{\bullet})_2\{P(OPh)_3\}]^+$ electronic configuration with an intermediate spin central ferric ion ($S_{Fe} = {}^3/_2$) coupled antiferromagnetically to two π-radical anions.

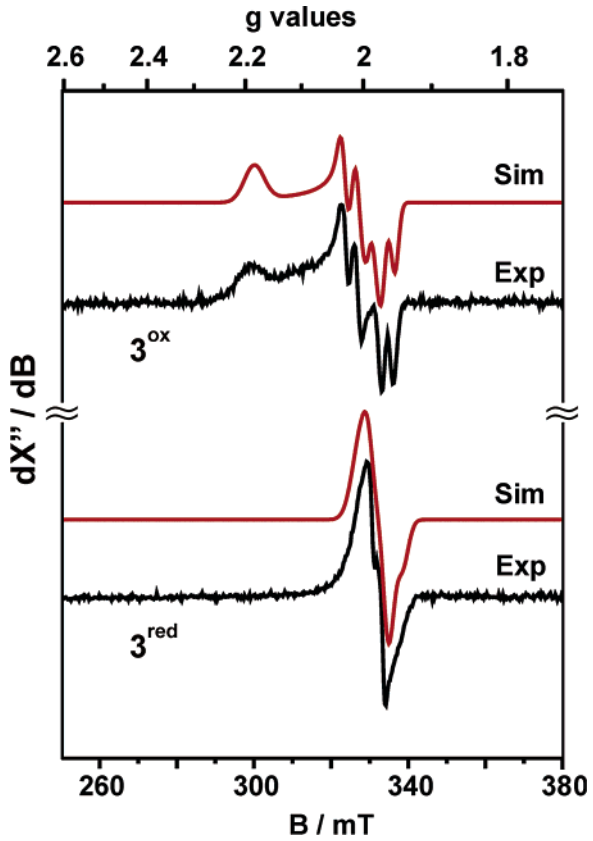

Figure 12. X-band EPR spectra of electrochemically generated **3**^{ox} (top) and **3**^{red} (bottom) in CH_2Cl_2 (0.10 M [N(*n*-Bu)$_4$]PF$_6$ at 10 K; frequency = 9.43 GHz, modulation = 10.0 G, power = 100 μW). For simulation parameters see text.

Table 4. Mössbauer Parameters of Complexes

	T	δ (mm s^{-1})^a	ΔE_Q (mm s^{-1})^b	S_t^{c}
1	80	0.11	−2.55	0
	4.2	0.11	−2.59	
1^{ox}	80	0.26 (50%)	1.93	1/2
	80	0.45 (40%)	0.53	3/2
	80	0.92 (10%)	2.87	?
	4.2	0.27 (58%)	1.94	1/2
	4.2	0.36 (30%)	0.59	3/2
	4.2	0.95 (12%)	2.93	?
	295	0.16 (30%)	1.97	1/2
	295	0.39 (70%)	0.65	3/2
1^{red}	80	0.33	2.18	1/2
2	4.2	0.21	+2.66	1/2
	80	0.21	2.63	
3	4.2	0.07	−2.69	0
	80	0.06	−2.69	
4	80	0.08	2.55	0
4^{ox}	80	0.25	1.74	1/2

^{a} Isomer shift vs α-Fe at 298 K. ^{b} Quadrupole splitting. ^{c} Ground state.

Mössbauer Spectroscopy. Solid samples of all complexes (Scheme 1) have been carefully investigated by zero-field Mössbauer spectroscopy at 80 K and applied field (1−7 T) at 4.2 K; detailed spin Hamilton analyses have been carried out. In addition, a zero-field Mössbauer spectrum of a frozen CH_2Cl_2 solution sample of **4**^{ox} was recorded at 80 K. The results are summarized in Table 4.

The zero- and applied field (7.0 T, 4.2) spectra of solid **1** are shown in Figure S2. The zero-field spectrum at 80 K displays two quadrupole doublets (area ratio 91:9) where the minority species is a high-spin ferric impurity ($\delta = 0.46$,

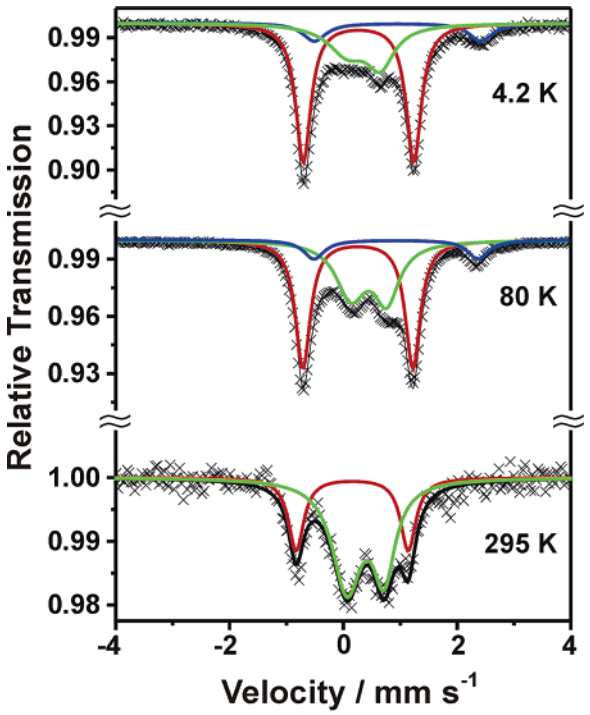

Figure 13. Zero-field Mössbauer spectra of $\mathbf{1}^{ox}$ at 4.2 K (top), 80 K (middle), and 295 K (bottom). The fits include three subspectra at 4.2 and 80 K but only two at 295 K. The parameters are given in Table 4.

$\Delta E_Q = 0.74$). The absence of an internal field in the applied field spectrum proves the $S_t = 0$ ground state of **1**. The low isomer shift δ of 0.11 mm s^{-1} and the large *negative* quadrupole splitting parameter of -2.59 mm s^{-1} at 4.2 K are quite typical for square-based pyramidal complexes containing a diamagnetic central ferrous ion ($S_{Fe} = 0$): $[Fe^{II}(^1L^\bullet)_2(CN)]^{1-}$ ($S_{Fe} = 0$, $S_t = 0$). Nearly identical isomer shift and quadrupole parameters have been found for **3**, $[Fe^{II}(^1L^\bullet)_2\{P(OCH_3)_3\}]^0$, and **4**, $[Fe^{II}(^3L)_2\{P(OPh)_3\}]^0$.

The zero-field spectrum of solid $\mathbf{1}^{ox}$ at 80 K shown in Figure 13 (middle) was readily deconvoluted into three quadrupole doublets (ratio 50:40:10) of which the 10% signal is caused by a high-spin ferrous impurity. The ratio of the other two signals is temperature dependent: at 4.2 K, the ratio is 58:30:12, and at room temperature, it is 30:70. This reflects the typical behavior of a gradual (incomplete) spin-crossover $S_t = {}^3/_2 \leftrightarrow S_t = {}^1/_2$ and is in full agreement with the susceptibility data shown in Figure 9.

If it is accepted that the doublet with the larger isomer shift at 0.45 mm s^{-1} at 80 K and the smaller quadrupole splitting at 0.5 mm s^{-1} originates from a high-spin ferric ion, then the other doublet ($\delta = 0.27$ mm s^{-1}, $\Delta E_Q = 1.94$ mm s^{-1}) stems from a compound with a central intermediate-spin ferric ion. Thus, $\mathbf{1}^{ox}$ has an electronic structure of $[Fe^{III}(^1L^\bullet)_2(CN)]^0$ ($S_{Fe} = {}^5/_2 \rightleftharpoons {}^3/_2$, $S_t = {}^3/_2 \rightleftharpoons {}^1/_2$). Similar behavior has been reported previously by us for $[Fe^{III}(L^\bullet_{N,O})_2Br]$, where again, a spin-crossover $S_t = {}^3/_2 \rightleftharpoons {}^1/_2$ has been observed and traced to an intrinsic spin-crossover at the ferric ion ($S_{Fe} = {}^5/_2 \rightleftharpoons {}^3/_2$).[20] $(L^\bullet_{N,O})^{1-}$ represents the monoanionic π radical[20,21] of the *o*-iminophenolate dianion.

Figure S3 displays the applied field spectrum (1, 4, 7 T at 4.2 K) of solid **2**; at 80 K, the zero-field spectrum shows a single quadrupole doublet (Table 4, not shown). The hyperfine parameters, $A_{xx}/g_N\beta_N = -14.39$ T, $A_{yy}/g_N\beta_N = -30.43$ T, $A_{zz}/g_N\beta_N = +0.97$ T, and $\langle A\rangle/g_N\beta_N = -14.61$ T, are very similar to those reported for the iodide complexes shown in Figure 11. The hallmarks of five-coordinate intermediate-spin ferric complexes are large quadrupole splittings ($\sim$3.0 mm s^{-1}), as well as two major negative components and a minor positive one of the *A* tensor.[20−23,36−39] For a more detailed discussion and data see Tables 6 and 7 in ref 23. Thus, the electronic structure of **2** is correctly described as $[Fe^{III}(^1L^\bullet)_2I]$ ($S_{Fe} = {}^3/_2$, $S_t = {}^1/_2$).

The Mössbauer parameters for $\mathbf{4}^{ox}$ at 80 K resemble closely those of $\mathbf{1}^{ox}$ ($S_t = {}^1/_2$) and **2**, and therefore, its electronic structure is best described as $[Fe^{III}(^3L^\bullet)_2\{P(OPh)_3\}]^+$ ($S_{Fe} = {}^3/_2$, $S_t = {}^1/_2$).

Finally, the zero-field Mössbauer spectrum of a frozen CH_2Cl_2 solution (0.10 M $[N(n\text{-}Bu)_4]PF_6$) of electrochemically generated $\mathbf{1}^{red}$ ($S_t = {}^1/_2$) has been recorded at 80 K (Figure S4). The isomer shift of $\delta = 0.33$ mm s^{-1} and the quadrupole splitting of $|\Delta E_Q| = 2.18$ mm s^{-1} could be seen in reasonable agreement with an electronic structure of $[Fe^{III}(^1L)_2(CN)]^{2-}$ containing an intermediate-spin ferric ion. This is clearly ruled out by the observed $S_t = {}^1/_2$ ground state. On the other hand, the parameters are not consistent with a five-coordinate low-spin ferric ion, which have never been found in this type of coordination chemistry. This implies that an electronic structure, such as $[Fe^{II}(^1L^\bullet)(^1L)(CN)]^{2-}$, with an intermediate-spin *ferrous* ion ($S_{Fe} = 1$) coupled antiferromagnetically to a π-radical ligand $(^1L^\bullet)^{1-}$ yielding the observed $S_t = {}^1/_2$ ground state could be more appropriate. We note that the square planar intermediate-spin complex $[Fe^{II}(L)_2]^{2-}$ has the following Mössbuer parameters at 80 K:[40] $\delta = 0.44$ mm s^{-1}, $|\Delta E_Q| = 1.20$ mm s^{-1}, $S_t = 1$ (L^{2-} = benzene-1,2-dithiolate). With the scarce data at hand for $\mathbf{1}^{red}$, for which the IR and UV−vis spectra indicate the presence of at least one delocalized ligand π radical, we favor the electronic structure description $[Fe^{II}(^1L^\bullet)(^1L)(CN)]^{2-} \leftrightarrow [Fe^{II}(^1L)(^1L^\bullet)(CN)]^{2-}$ ($S_{Fe} = 1$, $S_t = {}^1/_2$).

DFT-Calculations. Geometry optimization of the truncated monoanion, $[Fe(L)_2(CN)]^{1-}$, was carried out with the B3LYP functional. In the truncated model complex, the two *p*-*tert*-butylphenyl groups of the ligand $(^1L)^{n-}$ have been substituted by methyl groups. The resulting bond distances of the calculated and experimental structures are listed in Table 6.

No broken symmetry (BS) solution was found for this monoanion. Therefore, we report here the results for the closed-shell calculation only. The short average C−S distance

(36) Keutel, H.; Käpplinger, I.; Jäger, E.-G.; Grodzicki, M.; Schünemann, V.; Trautwein, A. X. *Inorg. Chem.* **1999**, *38*, 2320.
(37) Kostka, K. L.; Fox, B. G.; Hendrich, M. P. Collins, T. J.; Rickard, C. E.; Wright, L. J.; Münck, E. *J. Am. Chem. Soc.* **1993**, *115*, 6746.
(38) Koch, W. O.; Schünemann, V.; Gerdan, M.; Trautwein, A. X.; Krüger, H.-J. *Chem.—Eur. J.* **1998**, *4*, 686.
(39) (a) Gupta, G. P.; Lang, G.; Scheidt, W. R.; Geiger, D. K.; Reed, C. A. *J. Chem. Phys.* **1986**, *85*, 5212. (b) Gupta, G. P.; Lang, G.; Reed, C. A.; Shelly, K.; Scheidt, W. R.; Geiger, D. K. *J. Chem. Phys.* **1987**, *86*, 5288.
(40) Ray, K.; Begum, A.; Weyhermüller, T.; Piligkos, S.; Slageren, J.-V.; Neese, F.; Wieghardt, K. *J. Am. Chem. Soc.* **2005**, *127*, 4403.

Table 5. Classification, Spin States, and Mössbauer Parameters of Square-Based Pyramidal Iron Complexes[a]

	S_t	S_{Fe}	δ (mm s^{-1})	ΔE_Q (mm s^{-1})	ref
			Type I		
$[Fe^{III}(L^{\bullet}_{N,N})_2I]$	1/2	3/2	0.15	+3.03	21
$[Fe^{III}(L^{\bullet}_{N,N})_2(PBu_3)]^+$	1/2	3/2	0.06	+2.82	21
$[Fe^{III}(L^{\bullet}_{N,N})_2(Ph_2Im)]$	1/2	3/2	0.11	2.26	21
$[Fe^{III}(L^{\bullet}_{N,O})_2I]$	1/2	3/2	0.24	2.80	20a, b
$[Fe^{III}(L^{\bullet}_{N,O})_2Cl]$	3/2	5/2	0.45	1.26	20b
$[Fe^{III}(L^{\bullet}_{N,S})_2I]$	1/2	3/2	0.15	3.09	22
$[Fe^{III}(L^{\bullet}_{S,S})_2(PR_3)]^+$	1/2	3/2	0.25	2.60	23
1^{ox}, **2**, and **4**^{ox}	1/2	3/2			this work, see Table 4
			Type II		
$[Fe^{II}(L^{\bullet}_{N,N})_2(C{\equiv}NR)]$	0	0	0.10	2.64	21
$[Fe^{II}(L^{\bullet}_{N,N})_2(PBu_3)]$	0	0	0.13	2.96	21
$[Fe^{II}(L^{\bullet}_{N,S})_2(CN)]^{1-}$	0	0	0.05	2.98	22
$[Fe^{II}(L^{\bullet}_{N,S})_2\{P(OR)_3\}]$	0	0	0.06	2.92	22
$[Fe^{II}(mnt^{Y})_2\{PPh_3\}]$	0	0	0.12	2.78	6, 7
1, **3**, and **4**					this work, see Table 4
			Type III		
$[Fe^{III}(L^{\bullet}_{N,N})(L_{N,N})(BuPhCH\text{-}py)]$	1	3/2	0.20	+3.06	21
$[Fe^{III}(L^{\bullet}_{S,S})(L_{S,S})(Bu\text{-}py)]$	1	3/2	0.29	3.02	23
$[Fe^{III}(L_{S,S})(L^{\bullet}_{S,S})(PMe_3)]$	1	3/2	0.12	3.05	23
$[Fe^{III}(L_{S,S})(L^{\bullet}_{S,S})(PBu_3)]$	1	3/2	0.09	3.19	23
$[Fe^{III}(^2L^{\bullet})(^2L)]_2$	0	3/2	0.25	1.93	14
			Type IV		
$[Fe^{II}(^1L^{\bullet})(^1L)(CN)]^{2-}$ (**1**^{red})	1/2	1	0.33	2.18	this work
$[Fe^{II}(^3L)(^3L^{\bullet})(PPh_3)]^{1-}$	1/2	1	0.12	2.78	
			Type V		
$[Fe^{III}(L_{S,S})_2(Bu\text{-}py)]^{1-}$	3/2	3/2	0.33	3.03	23
$[Fe^{III}(mnt)_2(idzm^+)]^0$ (1.5 K)	3/2	3/2	0.33	2.48	11, 12
	1/2	1/2	0.53	3.10	
$[Fe^{III}(mnt)_2(py)]^{1-}$	3/2	3/2	0.33	2.41	12

[a] Abbreviations:

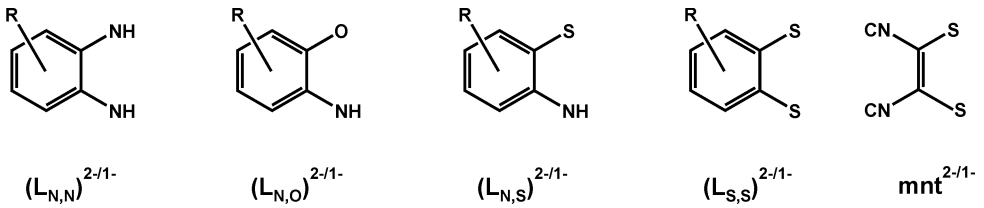

of 1.727 Å is in good agreement with the experiment (1.716 Å), and the experimental Fe−CN distance of 1.886 Å is well reproduced at 1.889 Å. The short average C−S bond length indicates the radical character of the dithiolate ligands, $(L^{\bullet})^{-1}$, as does the long average olefinic C−C bond at 1.38 Å.

The structure of the neutral paramagnetic complex $[Fe(L)_2(CN)]$ was optimized with the B3LYP functional using the standard open-shell Kohn−Sham approach and the broken symmetry method. For this complex, a BS solution with $M_s = {}^1/_2$ exists. The standard open-shell calculation ($M_s = {}^1/_2$) converged to the same solution as the BS one and will not be further distinguished. The adiabatic excitation energy for the BS model shows that the corresponding high-spin state is 28 kcal/mol less stable than the BS form.

It is interesting and significant that the calculated bond distances of the two dithiolate ligands in the truncated monoanion *and* its neutral analogue do not change. This is a clear indication that the oxidation level of the two dithiolate ligands remain the same upon oxidation of the monoanion to the neutral species. Only the Fe−C distances change from 1.888 Å in the monoanion to 1.972 Å in the neutral complex indicating less π back-donation in the latter oxidized species. Similarly, the average Fe−S distance at 2.212 Å in the monoanion *increases* to 2.253 Å in the neutral species. Thus, calculations show very clearly that the one-electron oxidation process is metal centered.

Electronic Structure. The molecular orbital scheme of the monoanion is shown in Figure 14. Three metal-centered d orbitals are found to be doubly occupied. The HOMO and LUMO are 83 and 70% ligand in character, respectively. In addition, there are two empty metal d orbitals above the LUMO. Thus, this occupation pattern implies the presence of an oxidation state of the metal center which is best described as low-spin Fe(II). Note that no significant covalent interaction (no π back-bonding) for the Fe−CN is detected.

In contrast, the molecular orbital scheme of neutral $[Fe(L)_2(CN)]$ as shown in Figure 15 displays one doubly occupied metal d orbital, three metal-based SOMOs, and an unoccupied Fe d orbital. Two of the metal SOMOs (d_{z^2} and d_{xz}) are coupled to two ligand-based orbitals via π pathways. This MO scheme indicates the presence of an intermediate-spin Fe(III) center coupled to two π-radical ligands. The spatial overlap of the corresponding orbitals[41] is strong ($S = 0.77$ and 0.57, respectively) which supports an antiferro-

(41) Neese, F. *J. Phys. Chem. Solids* **2004**, *65*, 781.

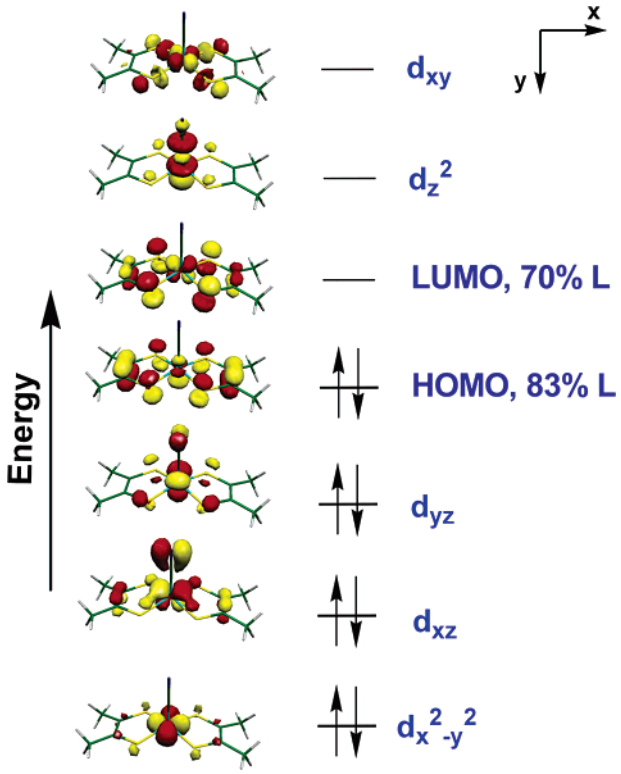

Figure 14. MO scheme for the monoanion $[Fe^{II}(^1L^{\bullet})_2(CN)]^-$.

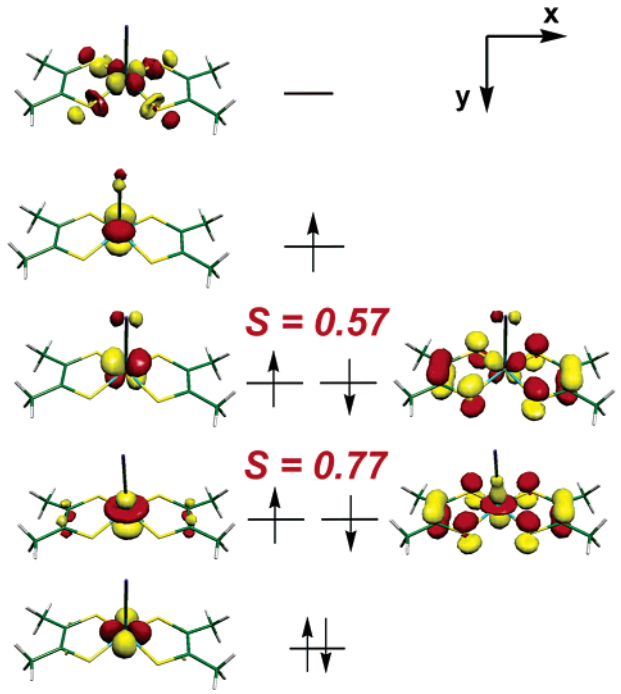

Figure 15. MO scheme for the neutral species $[Fe^{III}(^1L^{\bullet})_2(CN)]^0$.

magnetic coupling between the metal and the ligand. Indeed, calculation of the exchange coupling constant, J, according to the Yamaguchi approach,[42] yielded a strong antiferromagnetic coupling ($J = -1419$ cm^{-1} based on the Hamiltonian $\hat{H}_{HDvV} = -2J\hat{S}_A\hat{S}_B$).

The validity of the above electronic structural models for both iron complexes was checked by calculation of the Mössbauer parameters. The experimental Mössbauer isomer shift and quadrupole splitting of the $[Fe(L)_2(CN)]^{1-}$ complex ($\delta = 0.11$ mm s^{-1}, $\Delta E_Q = -2.59$ mm s^{-1}, $\eta = 0.48$) are in very good agreement with the computed Mössbauer values ($\delta = 0.16$ mm s^{-1}, $\Delta E_Q = -2.62$ mm s^{-1}, $\eta = 0.44$). An excellent agreement between theory and experiment has also been found for the neutral $[Fe(L)_2(CN)]$ complex; the experimental values of $\delta = 0.25$ mm s^{-1} and $\Delta E_Q = |1.93|$ mm s^{-1} match the calculated values at $\delta = 0.17$ mm s^{-1}, $\Delta E_Q = +2.05$ mm s^{-1}, and $\eta = 0.05$.

Thus, the electronic structures of the two complexes are correctly described by the above models.

Table 6. Calculated Bond Distances (Å) of $[Fe(L)_2(CN)]^{1-}$ and $[Fe(L)_2(CN)]$

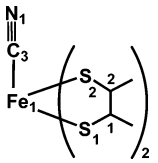

	$[Fe(L)_2(CN)]^{1-}$	$[Fe(L)_2(CN)]$
Fe1−C3	1.889	1.972
Fe1−S1	2.212	2.254
Fe1−S2	2.212	2.253
S1−C1	1.727	1.719
C1−C2	1.377	1.387
S2−C2	1.727	1.719
C3−N1	1.163	1.161

Discussion

In the following, we discuss the spectroscopic characteristics and structural markers for the five five-coordinate chromophores of iron (Table 5): (1) $[Fe^{III}(L^{\bullet})_2X]^n$, where X represents a monoanionic ligand (I^-, Cl^-, CN^-) and the charge $n = 0$ or X = neutral phosphine, phosphite, and $n = 1+$. The intrinsic spin state of the ferric ion is either $S_{Fe} = {}^5/_2$ or (in most cases) $S_{Fe} = {}^3/_2$, which affords an overall ground state of either $S_t = {}^3/_2$ or $S_t = {}^1/_2$. $(L^{\bullet})^{1-}$ represents a monoanionic π radical derived from *o*-phenylenediamine,[21] *o*-aminophenol,[20] *o*-aminobenzenethiol,[22] benzene-1,2-dithiol,[23] or the present series of 1,2-diaryl-ethylene-1,2-dithiolate ligands (Scheme 1). (2) $[Fe^{II}(L^{\bullet})_2X]^n$, where X^- is again an anion and $n = 1-$, or if it represents a neutral ligand, then $n = 0$. The ferrous ion possesses either an intrinsic spin state of $S_{Fe} = 0$ or $S_{Fe} = 1$, affording in both cases an $S_t = 0$ ground state. (3) $[Fe^{III}(L^{\bullet})(L)X]^n \leftrightarrow [Fe^{III}(L)(L^{\bullet})X]^n$, where X is a neutral ligand and $n = 0$, and the iron ion possesses an intermediate spin of $S_{Fe} = {}^3/_2$, which yields the ground state of $S_t = 1$ via antiferromagnetic coupling with an $(L^{\bullet})^{1-}$ radical. (4) $[Fe^{II}(L^{\bullet})(L)X]^n \leftrightarrow [Fe^{II}(L)(L^{\bullet})X]^n$, where X is an anion or neutral ligand with $n = 2-$ or $1-$, respectively. The ferrous ion possesses an intermediate spin of $S_{Fe} = 1$, yielding the ground state $S_t = {}^1/_2$ via antiferromagnetic coupling with one ligand radical. (5) $[Fe^{III}(L)_2X]$, where X represents a neutral or a monocationic ligand with $n =$

(42) Soda, T.; Kitagawa, Y.; Onishi, T.; Takano, Y.; Shigeta, Y.; Nagao, H.; Yoshioka, Y.; Yamaguchi, K. *Chem. Phys. Lett.* **2000**, *319*, 223. (b) Yamaguchi, K.; Takahara, Y.; Fueno, T. In *Applied Quantum Chemistry*; Smith, V. H., Ed.; Reidel: Dordrecht, The Netherlands, 1986; p 155.

1− and 0, respectively, and the ferric ion possesses an intermediate spin of $S_{Fe} = S_t = {}^3/_2$.

Type V Complexes. Complexes of type V (Table 5) possess an electronic structure comprising an intermediate-spin ferric ion ($S_{Fe} = {}^3/_2$), two closed-shell dithiolato(2−) ligands in the equatorial plane, and a neutral pyridine-derived fifth ligand in the apical position of a square-based pyramid. Two such complexes have recently been fully structurally characterized, namely, $[Fe^{III}(mnt)_2(idzm^+)]^0$ [11,12] and $[P(CH_3)Ph_3][Fe^{III}(L)_2(t\text{-Bu-py})]$,[23] where L^{2-} is benzene-1,2-dithiolate(2−) and t-Bu-py is 4-*tert*-butylpyridine.

The Mössbauer parameters are very similar and indicative of the intermediate-spin state, $S_{Fe} = S_t = {}^3/_2$, as has been discussed in detail in refs 20−23 and 36−39. Kahn's complex[11] is remarkable because a spin-crossover behavior at ∼1.5 K has been reported: $S_t = {}^3/_2 \rightleftharpoons S_t = {}^1/_2$. The fact that the isomer shift of the ${}^3/_2$ species at 0.33 mm s^{-1} increases to 0.53 mm s^{-1} for the $S_t = {}^1/_2$ species rules out, in our opinion, a low-spin ferric ion being observed <4 K. See for example Krüger's octahedral complex for which a similar spin crossover has been reported, namely for [Fe^{III}(N,N′-dimethyl-2,11-diaza[3.3]-2,6-pyridinophane)(1,2-benzenedithiolate)](ClO_4), where the isomer shift *decreases* from 0.37 mm s^{-1} for the $S_t = {}^3/_2$ species to 0.27 mm s^{-1} for the $S_t = {}^1/_2$ species.[38]

Type IV Complexes. It has been suggested by Kahn et al.[11,12] that replacement of the apical pyridine-type weak-field ligand by a strong-field ligand like cyanide or a phoshine in the above type V complexes would yield a low-spin configuration ($S_{Fe} = {}^1/_2 = S_t$). Complexes **1^{red}** and $[Fe(mnt)_2\{PPh_3\}]^{1-}$ [2] possess an $S_t = {}^1/_2$ ground state, but at least, **1^{red}** may be better described as $[Fe^{II}(^1L^\bullet)(^1L)(CN)]^{2-} \leftrightarrow [Fe^{II}(^1L)(^1L^\bullet)(CN)]^{2-}$ containing an intermediate-spin ferrous ion ($S_{Fe} = 1$) and a π-radical ligand ($S_{rad} = {}^1/_2$) which couple antiferromagnetically yielding the observed $S_t = {}^1/_2$ ground state. The presence of an $(^1L^\bullet)^{1-}$ π-radical anion in **1^{red}** is suggested by the observation of a ν(C=Ṡ) stretching mode at 1154 cm^{-1} and by intense absorption bands in the NIR which are assigned to ligand-to-ligand intervalence bands. Nevertheless, we assign the above electronic structure for **1^{red}** only tentatively because definitive structural characterization is lacking. The EPR spectrum of **1^{red}** (Figure 12) also rules out the presence of a low-spin ferric ion and two closed-shell $(^1L)^{2-}$ ligands because it displays a very narrow signal at $g = 2.03$ with weak nonresolved ^{31}P hyperfine coupling. Thus, $[Fe^{III}(^1L)_2(CN)]^{2-}$ ($S_{Fe} = S_t = {}^1/_2$) is not a viable possibility.

Type III Complexes. Complexes of the type $[Fe^{III}(L^\bullet)(L)X]^0 \leftrightarrow [Fe^{III}(L)(L^\bullet)X]^0$ containing a weak- or strong-field neutral ligand X, a semiquinone type monoanionic ligand π radical, a closed-shell dianion L^{2-} of the catecholate(2−) type, and an intermediate-spin ferric ion ($S_{Fe} = {}^3/_2$), affording an overall spin of $S_t = 1$, have not been identified in the present series of complexes containing 1,2-diphenyl-1,2-ethylenedithiolate ligands. The electronic structures of these complexes shown in Table 5 have been described in ref 21 in detail. It is therefore important to note that the dinuclear species $[(^2L^\bullet)Fe^{III}(^2L)_2Fe^{III}(^2L^\bullet)]$ containing two localized $(^2L^\bullet)^{1-}$ radical monoanions in terminal positions and two bridging $(^2L)^{2-}$ dianions has been structurally and spectroscopically characterized: two intermediate-spin ferric ions couple intramolecularly antiferromagnetically as well as the two $(^1L^\bullet)^{1-}$ radicals yielding an overall $S_t = 0$ ground state. The Mössbauer parameters for the $[Fe^{III}(^2L^\bullet)(^2L)X]$ chromophore and the electronic spectrum are very similar to those of the other type III complexes in Table 5.

Type II Complexes. Complexes of this type contain an $[Fe^{II}(L^\bullet)_2X]^n$ chromophore with two π-radical monoanionic ligands in the equatorial positions of a square-based pyramidal coordination polyhedron and a strong-field neutral isonitrile, phosphine, phosphite or an anion like cyanide in the apical position. The spin state of the central ferrous ion can either be $S_{Fe} = 0$ or $S_{Fe} = 1$ (intermediate spin). The spins of the two π-radical ligands couple either antiferromagnetically or with the intermediate-spin ferrous ion yielding, in both cases, the observed diamagnetic ground state ($S_t = 0$). From the DFT calculations, it is concluded that the central ferrous ion possesses an $S = 0$ ground state. The presence of two π-radical anions has also been proven by X-ray crystallography for $[Fe^{II}(L^\bullet_{N,N})_2(C{\equiv}N{-}R)]$, $[Fe^{II}(L^\bullet_{N,N})_2\{PBu_3\}]$, and $[Fe^{II}(L^\bullet_{N,S})_2\{P(OR)_3\}]$ (see Table 5).

It is quite remarkable that the presence of two π-radical monoanions can be deduced from the reported crystal structures[9,10] of $[Fe^{II}(^3L^\bullet)_2\{P(OCH_3)_3\}]$ and $[Fe^{II}(S_2C_2(CF_3)_2)^\bullet_2\{AsPh_3\}]$ as shown above. The data agree nicely with those found in diamagnetic square-planar $[M^{II}(^1L^\bullet)_2]$ (M = Ni, Pd, Pt).[15,16]

The electronic spectra of all of these species exhibit an intense ($\epsilon > 10^4$ M^{-1} cm^{-1}) ligand-to-ligand (LLCT) band at ∼700 nm. In the present case, this LLCT band has been observed for **1** at 723 nm ($\epsilon = 1.7 \times 10^4$ M^{-1} cm^{-1}), for **3** at 702 (2.4×10^4), and for **4** at 687 (1.8×10^4). Notably, in the electronic spectrum of $[Fe^{II}(^3L^\bullet)_2\{PPh_3\}]^0$ ($S_t = 0$), this LLCT band has been reported at 702 (1.5×10^4).[3]

Type I Complexes. These species contain an $[Fe^{III}(L^\bullet)_2X]^n$ chromophore with two π-radical monoanionic ligands in equatorial positions and an anionic ligand (mostly I^-, but also Br^- or Cl^-) or a neutral phosphine in the apical position which affords $n = 0$ and 1+, respectively. The spin state of the central iron ion is mostly $S_{Fe} = {}^3/_2$, and in some cases, it is high spin ($S_{Fe} = {}^5/_2$), but no case of a low spin configuration has been detected to date.[11] The resulting spin ground state of the molecules is $S_t = {}^1/_2$, in most cases or, rarely, $S_t = {}^3/_2$. Interestingly, for **1^{ox}** and $[Fe^{III}(L^\bullet_{N,O})_2Br]$, a spin-crossover behavior has been identified $S_t = {}^1/_2 \rightleftharpoons S_t = {}^3/_2$ ($S_{Fe} = {}^3/_2 \rightleftharpoons S_{Fe} = {}^5/_2$).[20] As shown in Figure 12, the EPR spectra of the iodo complexes are very similar and quite characteristic for the type I chromophore. The EPR spectra of **3^{ox}** and **4^{ox}** display characteristic ^{31}P hyperfine splittings. The electronic spectra of these species display two intense LLCT bands ($\epsilon > 0.5 \times 10^3$) at ∼500 and ∼650 nm. The presence of two π-radical ligands has, in most cases in Table 5, been unequivocally established crystallo-

graphically for *o*-aminophenol,[20] *o*-aminobenzenethiol,[22] and *o*-phenylenediamine[21] derivatives: $(L^{\bullet}_{N,O})^{1-}$, $(L^{\bullet}_{N,S})^{1-}$, and $(L^{\bullet}_{N,N})^{1-}$.

Conclusions

The most salient feature of the present study is the observation that classic ethylenedithiolato ligands, such as 1,2-diphenyl-1,2-ethylenedithiolate, 1,2-diperfluoromethyl-1,2-ethylenedithiolate, or maleonitriledithiolate, are redox noninnocent ligands which in coordination compounds exist in at least two oxidation levels, namely, the diamagnetic closed-shell dianionic form and the paramagnetic ($S_{rad} = {}^1/_2$) open-shell monoanionic form. This gives rise to four different electronic structures for square-based pyramidal iron complexes $[Fe(L)_2X]^n$, where X is a neutral or monoanionic ligand and $n = 1+$, 0, $1-$, or $2-$. In this respect, the chemistry parallels that of *o*-phenylenediamines, *o*-aminophenols, *o*-aminobenzenethiols, and, *o*-benzenedithiols for which the same iron complexes have been identified.[20−23]

Acknowledgment. We thank the Fonds der Chemischen Industrie for financial support, the A.v. Humboldt Foundation for a fellowship for A.K.P., and the EPSRC (U.K.) for a studentship (K.S).

Supporting Information Available: Additional spectroscopic details are given in Figure S1 showing the X-band EPR spectrum of $\mathbf{4^{ox}}$, Figures S2 and S4 showing the zero field Mössbauer spectra of solid samples of **1** and $\mathbf{1^{red}}$, and Figure S3 showing the applied field Mössbauer spectra of compound **2** at 1, 4, and 7 T. Crystallographic details and tabular material on positional and displacement parameters, bond length, and angles are available for compounds **1** and **4** in CIF format. This material is available free of charge via the Internet at http://pubs.acs.org.

IC061171T